Rotation–Vibration Motion of Pyramidal XY_3 Molecules Described in the Eckart Frame: The Calculation of Intensities with Application to NH_3

Sergei N. Yurchenko,[1] Walter Thiel,[1] Miguel Carvajal,[2]
Hai Lin[3] and Per Jensen[4]

[1]*Max-Planck-Institut für Kohlenforschung, Kaiser-Wilhelm-Platz 1, D-45470 Mülheim an der Ruhr, Germany*
[2]*Departamento de Fisica Aplicada, Facultad de Ciencias Experimentales, Avda. de las FF.AA. s/n, Universidad de Huelva, 21071, Huelva, Spain*
[3]*Department of Chemistry, University of Minnesota, 207 Pleasant Street SE, Minneapolis, MN 55455, USA*
[4]*FB C – Theoretische Chemie, Bergische Universität, D-42097 Wuppertal, Germany*

Abstract

We present a theoretical model, with accompanying computer program, for simulating rotation–vibration absorption spectra of XY_3 pyramidal molecules in isolated electronic states. The theoretical approach is based on a recent computational scheme for solving the rotation–vibration Schrödinger equation of such molecules variationally [S. N. Yurchenko, M. Carvajal, P. Jensen, H. Lin, J. Zheng, and W. Thiel, *Mol. Phys.*, 2005, **103**, 359], and it makes use of dipole moment surfaces calculated *ab initio*. We apply the theory to $^{14}NH_3$ and demonstrate that the theoretical results show good agreement with experimental findings.

Contents

ADVANCES IN QUANTUM CHEMISTRY, VOLUME 48
ISSN: 0065-3276 DOI: 10.1016/S0065-3276(05)48014-4

1. INTRODUCTION

In a very recent publication [1], we have presented a new model for the rotation–vibration motion of pyramidal XY_3 molecules, based on the Hougen–Bunker–Johns (henceforth: HBJ) approach [2] (see also Chapter 15, in particular Section 15.2, of Ref. [3]). In this model, inversion is treated as a large-amplitude motion in the HBJ sense, while the other vibrations are assumed to be of small amplitude; they are described by linearized stretching and bending coordinates. The rotation–vibration Schrödinger equation is solved variationally to determine rotation–vibration energies. The reader is referred to Ref. [1] for a complete description of the theoretical and computational details.

We have already made several applications of the new model. Prior to Yurchenko *et al.* [1], we reported high-level *ab initio* potential energy surfaces for the NH_3 electronic ground state together with variational calculations of the associated vibrational energies [4]. Analogous nuclear-motion calculations for PH_3 [5] were based on the *ab initio* potential energy surface of Wang *et al.* [6], which was refined [5] in a simultaneous least-squares fitting to *ab initio* data and experimentally derived vibrational term values. In Ref. [1] we extended the theoretical treatment of Refs. [4,5] to include rotation and described some technical improvements to the original model for the vibrational motion. The resulting model for rotation and vibration was tested in calculations for $^{14}NH_3$ using an analytical potential function derived from high-level *ab initio* calculations [1]. These test calculations produced the $J=0$ vibrational energies up to 6100 cm^{-1}, the $J \leq 2$ energies for the vibrational ground state and the ν_2, ν_4, and $2\nu_2$ excited vibrational states, and the $J \leq 7$ energies for the $4\nu_2^+$ vibrational state. The computed energies were found to be in very satisfactory agreement with the corresponding experimentally derived values, and superior in this regard to the results of other recent theoretical calculations [7,8].

The new model has also been applied to the calculation of thermally averaged probability density functions for the out-of-plane inversion motion of the CH_3^+ and H_3O^+ ions [9]. Such probability densities can be obtained experimentally by means of Coulomb Explosion Imaging (CEI) techniques (see, for example, Refs. [10,11]), and the results in Ref. [9] will be useful in the interpretation of the resulting images, just as analogous calculations of the bending probability distribution for the CH_2^+ ion were instrumental in the interpretation of its CEI images (see Refs. [9,12] and references therein).

Another application is concerned with highly excited rotational levels of the PH_3 molecule [13,14]. The calculations show that these rotational levels form near-degenerate six-fold energy clusters analogous to the four-fold clusters formed in triatomic dihydrides H_2X (see, for example, Refs. [3,15,16] and references therein).

One of the most important aims of our theoretical work is to assist in the interpretation and understanding of high-resolution molecular spectroscopy experiments. We have already been able [1] to provide assistance of this kind in that, with our calculated values for the rotational energies in the $4\nu_2^+$ vibrational state of $^{14}NH_3$, we could verify (and, for a few transitions, refute) the tentative assignment to the $4\nu_2^+$ band [17] of 55 weak transitions observed in an

experimental study of the ν_1, ν_3, and $2\nu_4$ bands of $^{14}NH_3$. To provide theoretical support for high-resolution molecular spectroscopy experiments it is not sufficient, however, to calculate only molecular rotation–vibration energies. It is highly desirable to predict also theoretical intensities so that spectra can be simulated. As discussed in Ref. [1], our approach to the computation of molecular rotation–vibration energies and wavefunctions can be applied to rotation–vibration states with high J values (e.g., up to $J \leq 80$ for PH_3 [14]) where alternative variational treatments (see, for example, Refs. [7,8]), which make use of a nuclear kinetic energy operator exact within the Born–Oppenheimer approximation, are no longer feasible. This advantage arises from the maximum separation of rotation and vibration inherently built into the HBJ theory that we employ. We can calculate the energies and wavefunctions for states with J values sufficiently high that realistic spectra can be simulated. In the present work, we describe the extension of our model to the computation of the *line strengths* that determine the intensities of electric dipole transitions within the electronic state under consideration. The derivation is guided by Jensen and Špirko [18,19] and by Chapter 14 of Ref. [3]. The line strengths are obtained from the rovibronic wavefunctions that we generate as described in Ref. [1], and from *ab initio* molecular dipole moment surfaces. With the computed line strengths we can simulate absorption spectra of XY_3 molecules if we assume that the absorbing molecules are in thermal equilibrium at a known absolute temperature. We can also simulate emission spectra if we know the non-thermal population distribution of the emitting molecules.

2. THEORETICAL INTENSITIES AND SELECTION RULES

2.1. Line strengths

The intensity of an electric dipole transition in absorption or emission depends, on one hand, on factors particular to the experiment measuring the intensity, e.g., the number density of molecules in the initial state of the transition and, for absorption experiments, the absorption path length and the intensity of the incident light. On the other hand, the intensity involves a factor independent of the experimental parameters. This factor, *the line strength* $S(\mathrm{f} \leftarrow \mathrm{i})$, determines the probability that a molecule in the initial state i of the transition $\mathrm{f} \leftarrow \mathrm{i}$ will end up in the final state f within unit time.

If we assume that the initial state i and the final state f are both non-degenerate, then the line strength of the electric dipole transition between them [3] is given by

$$S(\mathrm{f} \leftarrow \mathrm{i}) = \sum_{A=X,Y,Z} |\langle \Phi_\mathrm{f} | \mu_A | \Phi_\mathrm{i} \rangle|^2. \tag{1}$$

As in Ref. [1], we describe the molecule in a space-fixed (or laboratory-fixed) axis system XYZ, and μ_A is the component of the molecular dipole moment along the axis $A = X$, Y, or Z. The complete internal wavefunctions of the initial and final states are written as $|\Phi_\mathrm{i}\rangle$ and $|\Phi_\mathrm{f}\rangle$, respectively. In the present work, we take the

complete internal wavefunctions to be given as

$$|\Phi_{\rm w}\rangle = |\Phi_{\rm ns}^{\rm (w)}\rangle|\Phi_{\rm elec}^{\rm (w)}\rangle|\Phi_{\rm rv}^{\rm (w)}\rangle, \tag{2}$$

where w = i or f. We can separate out the nuclear spin wavefunction $|\Phi_{\rm ns}^{\rm (w)}\rangle$ [3] because we assume the molecular energies to be independent of nuclear spin (i.e., we neglect *hyperfine structure*). The remaining factorization into a product of an electronic wavefunction $|\Phi_{\rm elec}^{\rm (w)}\rangle$ and a rotation–vibration wavefunction $|\Phi_{\rm rv}^{\rm (w)}\rangle$ follows from the Born–Oppenheimer approximation (see, for example, Ref. [3]) which we assume to be valid.

Inserting the wavefunction from equation (2) in the matrix element square of equation (1), we obtain

$$|\langle\Phi_{\rm f}|\mu_A|\Phi_{\rm i}\rangle|^2 = |\langle\Phi_{\rm ns}^{\rm (f)}|\Phi_{\rm ns}^{\rm (i)}\rangle|^2|\langle\Phi_{\rm rv}^{\rm (f)}\Phi_{\rm elec}^{\rm (f)}|\mu_A|\Phi_{\rm elec}^{\rm (i)}\Phi_{\rm rv}^{\rm (i)}\rangle|^2 \tag{3}$$

where we have made use of the fact that the dipole moment component μ_A does not depend on the nuclear spin. The nuclear spin functions are orthogonal and normalized. Consequently, the integral on the left-hand side of equation (3) vanishes unless $|\Phi_{\rm ns}^{\rm (f)}\rangle = |\Phi_{\rm ns}^{\rm (i)}\rangle$ so that $|\langle\Phi_{\rm ns}^{\rm (f)}|\Phi_{\rm ns}^{\rm (i)}\rangle|^2 = 1$.

As mentioned above, we assume that the molecular energy does not depend on the nuclear spin state $|\Phi_{\rm ns}^{\rm (w)}\rangle$. For the initial rovibronic state $|\Phi_{\rm elec}^{\rm (i)}\rangle|\Phi_{\rm rv}^{\rm (i)}\rangle$, we have $g_{\rm ns}$ nuclear spin functions $|\Phi_{\rm ns}^{\rm (i)}\rangle$ available, for which the product function $|\Phi_{\rm i}\rangle$ in equation (2) is an allowed complete internal state for the molecule in question, because it obeys Fermi–Dirac statistics by permutations of identical fermion nuclei, and Bose–Einstein statistics by permutations of identical boson nuclei (see Chapter 8 in Ref. [3]). By necessity [3], the same $g_{\rm ns}$ nuclear spin functions can be combined with the final rovibronic state $|\Phi_{\rm elec}^{\rm (f)}\rangle|\Phi_{\rm rv}^{\rm (f)}\rangle$ to form allowed complete internal states $|\Phi_{\rm f}\rangle$. The quantity $g_{\rm ns}$ is referred to as the *nuclear spin statistical weight factor.*

In our approximation, the upper and lower states of the transition f ← i are both $g_{\rm ns}$-fold degenerate owing to the availability of the $g_{\rm ns}$ 'allowed' nuclear spin functions. Furthermore, they have *m-degeneracy* since for a molecule in field-free space, the energy does not depend on m, the projection of the total angular momentum on the Z axis. We denote the m value of the initial state as $m_{\rm i}$ and that of the final state as $m_{\rm f}$. In the calculation of the line strength, we account for the nuclear spin degeneracy and the m-degeneracy by generalizing equation (1) to

$$S({\rm f} \leftarrow {\rm i}) = g_{\rm ns} \sum_{m_{\rm f}, m_{\rm i}} \sum_{A=X,Y,Z} |\langle\Phi_{\rm rv}^{\rm (f)}\Phi_{\rm elec}^{\rm (f)}|\mu_A|\Phi_{\rm elec}^{\rm (i)}\Phi_{\rm rv}^{\rm (i)}\rangle|^2 \tag{4}$$

where we have made use of equation (3) with $|\langle\Phi_{\rm ns}^{\rm (f)}|\Phi_{\rm ns}^{\rm (i)}\rangle|^2 = 1$.

2.2. Intensities

If, in an absorption experiment, a parallel beam of light at wavenumber $\tilde{\nu}$ with intensity $I_0(\tilde{\nu})$ passes through a length l of gas at a concentration of $c_{\rm g}$, the intensity of the transmitted light $I_{\rm tr}(\tilde{\nu})$ is given by the Lambert–Beer law

$$I_{tr}(\tilde{\nu}) = I_0(\tilde{\nu}) \exp[-lc_g\varepsilon(\tilde{\nu})] \tag{5}$$

where $\varepsilon(\tilde{\nu})$ is the absorption coefficient. By integrating the absorption coefficient over an absorption line one obtains the expression

$$I(\mathrm{f} \leftarrow \mathrm{i}) = \int_{\text{Line}} \varepsilon(\tilde{\nu})\, \mathrm{d}\tilde{\nu} = \frac{8\pi^3 N_A \tilde{\nu}_{if}}{(4\pi\varepsilon_0)3hc} \frac{e^{-E_i/kT}}{Q} [1 - \exp(-hc\tilde{\nu}_{if}/kT)] S(\mathrm{f} \leftarrow \mathrm{i}) \tag{6}$$

for the intensity of the absorption line for the transition from the state i with energy E_i, in thermal equilibrium at the temperature T, to the state f with energy E_f, where $hc\tilde{\nu}_{if} = E_f - E_i$, N_A is the Avogadro constant, h is Planck's constant, c is the speed of light in vacuum, k is the Boltzmann constant, ε_0 is the permittivity of free space, $S(\mathrm{f} \leftarrow \mathrm{i})$ is the line strength defined in equation (4), and, finally, Q is the partition function defined as

$$Q = \sum_j g_j\, e^{-E_j/kT}, \tag{7}$$

where g_j is the total degeneracy of the state with energy E_j and the sum runs over all energy levels of the molecule.

The 'molecule-intrinsic' factor in the intensities of emission spectra can be obtained from the well-known Einstein coefficients (see, for example, Refs. [20, 21]). For the two states i and f considered above, whose energies are E_i and E_f, respectively, with $E_i < E_f$, we define B_{if} as the Einstein coefficient for absorption, B_{fi} as the Einstein coefficient for stimulated emission, and A_{fi} as the Einstein coefficient for spontaneous emission. We denote by N_i and N_f the number of molecules with energies E_i and E_f, respectively, and the Einstein coefficients are defined such that, for example, the change in N_f caused by electric dipole transitions to and from i is given by

$$\frac{\mathrm{d}N_f}{\mathrm{d}t} = \rho(\nu)[N_i B_{if} - N_f B_{fi}] - N_f A_{fi}. \tag{8}$$

The energy density function $\rho(\nu)$ is defined so that $\mathrm{d}E = \rho(\nu)\mathrm{d}\nu$ is the amount of available radiation energy per unit volume originating in radiation with *frequency* in the infinitesimal interval $[\nu, \nu + \mathrm{d}\nu]$. Thus, $\rho(\nu)$ is expressed in the SI units $\mathrm{J/(m^3\ Hz) = J\ s/m^3}$, so that B_{fi} and B_{fi} have the SI units $\mathrm{m^3/(J\ s^2)}$. A_{fi} is expressed in $\mathrm{s^{-1}}$. The Einstein coefficients defined in this manner are related to the line strength by

$$g_i B_{if} = g_f B_{fi} = \frac{8\pi^3}{3h^2(4\pi\varepsilon_0)} S(\mathrm{f} \leftarrow \mathrm{i}) \tag{9}$$

and

$$g_f A_{fi} = \frac{64\pi^4}{3h(4\pi\varepsilon_0)} \tilde{\nu}_{if}^3 S(\mathrm{f} \leftarrow \mathrm{i}), \tag{10}$$

where g_i and g_f are the total degeneracies of the states i and f, respectively.

Sometimes an alternative definition of the Einstein coefficients is employed. With this definition, equation (8) is replaced by

$$\frac{dN_f}{dt} = \tilde{\rho}(\tilde{\nu})[N_i\tilde{B}_{if} - N_f\tilde{B}_{fi}] - N_f\tilde{A}_{fi}. \tag{11}$$

where $\tilde{\rho}(\tilde{\nu})$ is defined so that $dE = \tilde{\rho}(\tilde{\nu})d\tilde{\nu}$ is the amount of available radiation energy per unit volume originating in radiation with *wavenumber* in the infinitesimal interval $[\tilde{\nu}, \tilde{\nu} + d\tilde{\nu}]$. We have $\tilde{\rho}(\tilde{\nu}) = c\rho(\tilde{\nu}c) = c\rho(\nu)$ together with $\tilde{B}_{if} = B_{if}/c$, $\tilde{B}_{fi} = B_{fi}/c$, and $\tilde{A}_{fi} = A_{fi}$. The SI units for $\tilde{\rho}(\tilde{\nu})$ are $J/(m^3\ m^{-1}) = J/m^2$, and those of $\tilde{B}_{if}$ and $\tilde{B}_{fi}$ are $m^2/(J\ s)$.

2.3. A detailed expression for the line strength

In the present section, we obtain an expression for the line strength in equation (4) in a form suitable for numerical calculation. This derivation closely follows the theory developed in Refs. [18,19] and in Chapter 14 of Ref. [3], and so we give only an outline here.

As discussed in Ref. [1], we describe the rotation of the molecule by means of a molecule-fixed axis system *xyz* defined in terms of Eckart and Sayvetz conditions (see Ref. [1] and references therein). The orientation of the *xyz* axis system relative to the *XYZ* system is defined by the three standard Euler angles (θ, ϕ, χ) [1]. To simplify equation (4), we must first express the space-fixed dipole moment components (μ_X, μ_Y, μ_Z) in this equation in terms of the components (μ_x, μ_y, μ_z) along the molecule-fixed axes. This transformation is most easily done by rewriting the dipole moment components in terms of so-called irreducible spherical tensor operators. In the notation in Ref. [3], the space-fixed irreducible tensor operators are

$$\mu_s^{(1,\pm1)} = \frac{1}{\sqrt{2}}(\mp\mu_X - i\mu_Y) \quad \text{and} \quad \mu_s^{(1,0)} = \mu_Z \tag{12}$$

with analogous expressions for the molecule-fixed operators

$$\mu_m^{(1,\pm1)} = \frac{1}{\sqrt{2}}(\mp\mu_x - i\mu_y) \quad \text{and} \quad \mu_m^{(1,0)} = \mu_z. \tag{13}$$

It can be shown that the space-fixed components are given in terms of the molecule-fixed components by equations (14) and (15) of Ref. [3]:

$$\mu_s^{(1,\sigma)} = \sum_{\sigma'=-1}^{1} [D^{(1)}_{\sigma\sigma'}(\phi, \theta, \chi)]^* \mu_m^{(1,\sigma')} \tag{14}$$

where $D^{(1)}_{\sigma\sigma'}(\phi, \theta, \chi)$ is an element of the standard rotation matrices given, for example, by Zare [22].

By inverting equation (12) to obtain (μ_X, μ_Y, μ_Z) and inserting the result in equation (4), we find that

$$S(\mathrm{f} \leftarrow \mathrm{i}) = g_{\mathrm{ns}} \sum_{m_\mathrm{f}, m_\mathrm{i}} \sum_{\sigma=-1}^{1} |\langle \Phi_{\mathrm{rv}}^{(\mathrm{f})} \Phi_{\mathrm{elec}}^{(\mathrm{f})} | \mu_{\mathrm{s}}^{(1,\sigma)} | \Phi_{\mathrm{elec}}^{(\mathrm{i})} \Phi_{\mathrm{rv}}^{(\mathrm{i})} \rangle|^2 \tag{15}$$

and we can now insert equation (14) in this expression. Simultaneously, we insert the expressions for the initial and final rotation–vibration wavefunctions $|\Phi_{\mathrm{rv}}^{(\mathrm{w})}\rangle$ from equation (67) of Ref. [1]:

$$|\Phi_{\mathrm{rv}}^{(\mathrm{i})}\rangle = \sum_{V'' K'' \tau_{\mathrm{rot}}''} C_{V'' K'' \tau_{\mathrm{rot}}''} |V''\rangle |J'' K'' m_\mathrm{i} \tau_{\mathrm{rot}}''\rangle; \quad K'' \geq 0 \tag{16}$$

$$|\Phi_{\mathrm{rv}}^{(\mathrm{f})}\rangle = \sum_{V' K' \tau_{\mathrm{rot}}'} C_{V' K' \tau_{\mathrm{rot}}'} |V'\rangle |J' K' m_\mathrm{f} \tau_{\mathrm{rot}}'\rangle; \quad K' \geq 0 \tag{17}$$

where $C_{V'' K'' \tau_{\mathrm{rpt}}''}$ and $C_{V' K' \tau_{\mathrm{rot}}'}$ are the expansion coefficients obtained as eigenvector components in the diagonalization of the Hamiltonian matrix [1], and the vibrational basis functions $|V\rangle$ are

$$|V\rangle = |n_1\rangle |n_2\rangle |n_3\rangle |n_\mathrm{b}, l_\mathrm{b}, \tau_{\mathrm{bend}}\rangle |n_\mathrm{i}, J, K, \tau_{\mathrm{inv}}\rangle; \tag{18}$$

V is used as a shorthand notation for all the quantum numbers and symmetry labels n_1, n_2, n_3, n_b, l_b, τ_{bend}, n_i, and τ_{inv} that label the vibrational basis functions. All the functions $|JKm\tau_{\mathrm{rot}}\rangle$, $|n_1\rangle$, $|n_2\rangle$, $|n_3\rangle$, $|n_\mathrm{b}, l_\mathrm{b}, \tau_{\mathrm{bend}}\rangle$, and $|n_\mathrm{i}, J, K, \tau_{\mathrm{inv}}\rangle$ occurring in equations (16)–(18), and the quantum numbers labelling them, are defined in detail in Ref. [1]: $|JKm\tau_{\mathrm{rot}}\rangle$ is a symmetrized rotational wavefunction defined in equations (68) and (69) of Ref. [1], $|n_1\rangle$, $|n_2\rangle$, and $|n_3\rangle$ are one-dimensional Morse oscillator eigenfunctions describing the stretching motion of the XY_3 molecule, $|n_\mathrm{b}, l_\mathrm{b}, \tau_{\mathrm{bend}}\rangle$ is a symmetrized eigenfunction of the two-dimensional harmonic oscillator modelling the small-amplitude bending motion, and $|n_\mathrm{i}, J, K, \tau_{\mathrm{inv}}\rangle$ is a symmetrized inversion basis function obtained by numerical solution of a zero-order inversion Schrödinger equation. Concerning the quantum numbers, it suffices to say here that each of the three quantum numbers τ_{rot}, τ_{bend}, and τ_{inv} assumes the values 0 or 1 in such a way that the parity (see below) of $|JKm\tau_{\mathrm{rot}}\rangle$ is $(-1)^{\tau_{\mathrm{rot}}}$, the parity of $|n_\mathrm{b}, l_\mathrm{b}, \tau_{\mathrm{bend}}\rangle$ is $(-1)^{\tau_{\mathrm{bend}}}$, and the parity of $|n_\mathrm{i}, J, K, \tau_{\mathrm{inv}}\rangle$ is $(-1)^{\tau_{\mathrm{inv}}}$.

Insertion of equations (14), (16), and (17) in equation (15) produces

$$\begin{aligned} S(\mathrm{f} \leftarrow \mathrm{i}) = g_{\mathrm{ns}} \sum_{m_\mathrm{i}, m_\mathrm{f}} \sum_{\sigma=-1}^{1} \Bigg| & \sum_{V' K' \tau_{\mathrm{rot}}'} \sum_{V'' K'' \tau_{\mathrm{rot}}''} C_{V' K' \tau_{\mathrm{rot}}'}^{*} C_{V'' K'' \tau_{\mathrm{rot}}''} \\ & \times \sum_{\sigma'=-1}^{1} \langle V' | \langle \Phi_{\mathrm{elec}}^{(\mathrm{f})} | \mu_{\mathrm{m}}^{(1,\sigma')} | \Phi_{\mathrm{elec}}^{(\mathrm{i})} \rangle | V'' \rangle \\ & \times \langle J' K' m_\mathrm{f} \tau_{\mathrm{rot}}' | [D_{\sigma\sigma'}^{(1)}(\phi, \theta, \chi)]^{*} | J'' K'' m_\mathrm{i} \tau_{\mathrm{rot}}'' \rangle \Bigg|^2 . \end{aligned} \tag{19}$$

We have factorized the matrix element in equation (19) by making use of the fact that the vibrational basis functions $|V''\rangle$ and $|V'\rangle$, the electronic wavefunctions $|\Phi_{\mathrm{elec}}^{(\mathrm{i})}\rangle$ and $|\Phi_{\mathrm{elec}}^{(\mathrm{f})}\rangle$, and the molecule-fixed dipole moment operator $\mu_{\mathrm{m}}^{(1,\sigma')}$ depend

on the vibrational and electronic coordinates only (these coordinates are defined in Ref. [1]), whereas the functions $|J'K'm_f\tau'_{rot}\rangle$, $|J''K''m_i\tau''_{rot}\rangle$, and $[D^{(1)}_{\sigma\sigma'}(\phi,\theta,\chi)]^*$ depend solely on the Euler angles (θ, ϕ, χ).

In the present work, we are only concerned with transitions within one electronic state so we have $|\Phi^{(f)}_{elec}\rangle = \Phi^{(i)}_{elec}\rangle$. We define the electronically averaged dipole moment operators

$$\bar{\mu}_m^{(1,\sigma')} = \langle \Phi^{(i)}_{elec} | \mu_m^{(1,\sigma')} | \Phi^{(i)}_{elec} \rangle_{el}; \tag{20}$$

the subscript 'el' signifies that in the matrix element, integration is over the electronic coordinates only so that $\bar{\mu}_m^{(1,\sigma')}$ is a function of the vibrational coordinates. We intend to obtain the $\bar{\mu}_m^{(1,\sigma')}$ functions from *ab initio* calculations as described in Section 3. By inserting equation (20) in equation (19); using equations (68) and (69) from Ref. [1] in conjunction with equation (14–23) from Ref. [3] to obtain analytical expressions for the integral involving $|J'K'm_f\tau'_{rot}\rangle$, $|J''K''m_i\tau''_{rot}\rangle$, and $[D^{(1)}_{\sigma\sigma'}(\phi,\theta,\chi)]^*$; and carrying out a significant amount of tedious algebra (using the results in Chapter 14 of Ref. [3]), we obtain the following expression for the line strength:

$$\begin{aligned}
S(f \leftarrow i) = g_{ns}(2J'+1)(2J''+1) \Bigg| & \sum_{V'K'\tau'_{rot}} \sum_{V''K''\tau''_{rot}} C^*_{V'K'\tau'_{rot}} C_{V''K''\tau''_{rot}} (i)^{\tau''_{rot}-\tau'_{rot}} \\
& \times \Bigg\{ \delta_{K'K''} \frac{1}{2} (-1)^{\sigma'_{rot}+\sigma''_{rot}+K'} (1+(-1)^{\tau'_{rot}+\tau''_{rot}+1}) \\
& \times \begin{pmatrix} J'' & 1 & J' \\ K'' & 0 & -K' \end{pmatrix} \langle V' | \bar{\mu}_m^{(1,0)} | V'' \rangle + [(\sqrt{2}-1)\delta_{K''0}+1] \\
& \times \delta_{K',K''+1} \frac{1}{2} (-1)^{\sigma'_{rot}+\sigma''_{rot}+K'} \begin{pmatrix} J'' & 1 & J' \\ K'' & 1 & -K' \end{pmatrix} \\
& \times [\langle V' \bar{\mu}_m^{(1,+1)} | V'' \rangle + (-1)^{\tau'_{rot}+\tau''_{rot}} \langle V' | \bar{\mu}_m^{(1,-1)} | V'' \rangle] \\
& + [(\sqrt{2}-1)\delta_{K'0}+1] \delta_{K',K''-1} \frac{1}{2} (-1)^{\sigma'_{rot}+\sigma''_{rot}+K'} \\
& \times \begin{pmatrix} J'' & 1 & J' \\ K'' & -1 & -K' \end{pmatrix} [\langle V' | \bar{\mu}_m^{(1,-1)} | V'' \rangle \\
& + (-1)^{\tau'_{rot}+\tau''_{rot}} \langle V' | \bar{\mu}_m^{(1,+1)} | V'' \rangle] \Bigg\} \Bigg|^2
\end{aligned} \tag{21}$$

where quantities such as

$$\begin{pmatrix} J'' & 1 & J' \\ K'' & -1 & -K' \end{pmatrix}$$

are standard 3*j*-symbols [3,22] and σ_{rot} is defined as

$$\sigma_{\text{rot}} = \begin{cases} K \bmod 3 & \text{for } \tau_{\text{rot}} = 1 \\ 0 & \text{for } \tau_{\text{rot}} = 0. \end{cases} \tag{22}$$

With the phase choices made for the basis functions in the present work, we obtain the real, positive line strength in equation (21) in the form $|is|^2$, where s is real, that is, as the module square of a purely imaginary number.

The *ab initio* calculations provide us with the Cartesian components of the dipole moment in the molecule-fixed axis system:

$$\bar{\mu}_\alpha = \langle \Phi^{(i)}_{\text{elec}} | \mu_\alpha | \Phi^{(i)}_{\text{elec}} \rangle_{\text{el}}, \quad \alpha = x, y, \text{ or } z, \tag{23}$$

and we obtain the vibrational matrix elements required in equation (21) from

$$\langle V' | \bar{\mu}^{(1,0)}_{\text{m}} | V'' \rangle = \langle V' | \bar{\mu}_z | V'' \rangle \tag{24}$$

together with

$$\langle V' | \bar{\mu}^{(1,+1)}_{\text{m}} | V'' \rangle + (-1)^{\tau'_{\text{rot}} + \tau''_{\text{rot}}} \langle V' | \bar{\mu}^{(1,-1)}_{\text{m}} | V'' \rangle$$

$$= -\frac{1}{\sqrt{2}} ([1 - (-1)^{\Delta\tau_{\text{rot}}}] \langle V' | \bar{\mu}_x | V'' \rangle + \text{i}[1 + (-1)^{\Delta\tau_{\text{rot}}}] \langle V' | \bar{\mu}_y | V'' \rangle), \tag{25}$$

where $\Delta\tau_{\text{rot}} = \tau'_{\text{rot}} - \tau''_{\text{rot}}$, and

$$\langle V' | \bar{\mu}^{(1,-1)}_{\text{m}} | V'' \rangle + (-1)^{\tau'_{\text{rot}} + \tau''_{\text{rot}}} \langle V' | \bar{\mu}^{(1,+1)}_{\text{m}} | V'' \rangle$$

$$= \frac{1}{\sqrt{2}} ([1 - (-1)^{\Delta\tau_{\text{rot}}}] \langle V' | \bar{\mu}_x | V'' \rangle - \text{i}[1 + (-1)^{\Delta\tau_{\text{rot}}}] \langle V' | \bar{\mu}_y | V'' \rangle). \tag{26}$$

We note that on the right-hand side of equations (25) and (26), the terms involving $\langle V' | \bar{\mu}_x | V'' \rangle$ and $\langle V' | \bar{\mu}_y | V'' \rangle$ are never simultaneously non-vanishing.

2.4. Symmetry and selection rules

For the XY_3 molecules considered here, we employ the Molecular Symmetry Group (MS group) $D_{3h}(\text{M})$ [3], given as the direct product [3],

$$D_{3h}(\text{M}) = C_{3v}(\text{M}) \otimes \{E, E^*\} \tag{27}$$

where E is the identity operation, E^* is the inversion operation which inverts all particles in the molecular centre of mass [3], and the group

$$C_{3v}(\text{M}) = \{E, (123), (132), (12)^*, (13)^*, (23)^*\}. \tag{28}$$

Here, (123) and (132) are cyclic permutations of the three Y nuclei (labelled 1, 2, 3) in XY_3 and each of the permutation-inversion operations $(12)^*$, $(13)^*$, and $(23)^*$ involves the interchange of two of the Y nuclei and the inversion operation E^* [3]. The character table of $D_{3h}(\text{M})$ is given in Table 1. The Complete Nuclear

Table 1. The character table of the MS group D_{3h}(M) [3]

	E	(123)	(23)	E^*	$(123)^*$	$(23)^*$	
	1	2	3	1	2	3	
A'_1	1	1	1	1	1	1	$(r_1+r_2+r_3)/\sqrt{3}$, $1/\sqrt{3}(\alpha_1+\alpha_2+\alpha_3)$, $\sin\rho$, Γ_B^+
A''_1	1	1	1	−1	−1	−1	Γ^*, Γ_B^-
A'_2	1	1	−1	1	1	−1	$\hat{J}_z$, Γ_F^+
A''_2	1	1	−1	−1	−1	1	$\cos\rho$, $\hat{J}_\rho$, $\bar{\mu}_z$, Γ_F^-
E'	2	−1	0	2	−1	0	$([2r_1-r_2-r_3]/\sqrt{6}$, $[r_2-r_3]/\sqrt{2})$, $([2\alpha_1-\alpha_2-\alpha_3]/\sqrt{6}$, $[\alpha_2-\alpha_3]/\sqrt{2}),(\bar{\mu}_x,\bar{\mu}_y)$
E''	2	−1	0	−2	1	0	$(\hat{J}_x,\hat{J}_y)$

Permutation Inversion (CNPI) Group [3], which contains all possible permutation-inversion operations [3] for a given molecule, has 24 elements for the XY_3 molecule, and the 12-member group D_{3h}(M) is obtained by deleting from the CNPI group the 12 *unfeasible* [3] symmetry operations that, when applied to an initial molecular geometry, take the molecule into a new geometry that can only be reached from the initial one by the breaking and reformation of bonds. We assume that the breaking and reformation of bonds are associated with energy barriers so large that this type of motion does not take place on the typical timescale of the spectroscopy experiments whose results we simulate.

The MS group D_{3h}(M) is obviously appropriate for planar XY_3 molecules such as CH_3^+ and for 'floppy' molecules like NH_3 with a pyramidal, non-planar equilibrium configuration but a barrier to planarity so low that tunnelling through the barrier is facile already at room temperature. For pyramidal molecules with a high barrier to planarity, such as PH_3, the appropriate MS group is C_{3v}(M) in equation (28).

In Table 1, we give for each class of D_{3h}(M) a representative element and the number of elements in the class. Also, we indicate the D_{3h}(M) symmetries of some quantities of interest: ρ is the HBJ inversion coordinate [1] (see also Fig. 1) and $\hat{J}_\rho$ is its conjugate momentum, $(\hat{J}_x,\hat{J}_y,\hat{J}_z)$ are the components of the total angular momentum along the molecule-fixed xyz axes, $(\bar{\mu}_x,\bar{\mu}_y,\bar{\mu}_z)$ are the electronically averaged dipole moment components along the molecule-fixed axes (see below), (r_1, r_2, r_3) are the instantaneous values of the bond lengths of the XY_3 molecule, while $\alpha_1=\angle(Y_2XY_3)$, $\alpha_2=\angle(Y_1XY_3)$, and $\alpha_3=\angle(Y_1XY_2)$ are the three bond angles (Y_i is the Y nucleus labelled $i=1,2,3$). The irreducible representation $\Gamma^*=A''_1$ is the so-called *electric dipole representation*; it has character +1 under each of the permutation operations in D_{3h}(M) and character −1 under each of the permutation-inversion operations. It is required for determining the symmetry selection rules for electric dipole transitions. Finally, the two irreducible representations $\Gamma_F^+=A'_2$ and $\Gamma_F^-=A''_2$ are the Pauli-allowed symmetries for NH_3

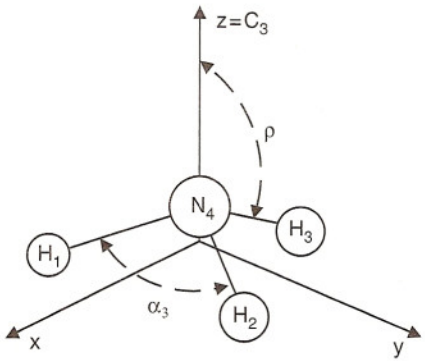

Fig. 1. The geometrically defined coordinates and the labelling of the nuclei chosen for NH^3.

(or for a general XY_3 molecule whose Y nuclei are fermions): Owing to Fermi–Dirac statistics, the complete internal wavefunctions of NH_3 must transform as A_2' or A_2'' in D_{3h}(M). Complete internal wavefunctions of NH_3 with A_2' symmetry have $+$ *parity* in that they have a character of $+1$ under the inversion operation E^*; those with A_2'' symmetry have $-$ *parity*, i.e., a character of -1 under E^*. The irreducible representations $\Gamma_B^+ = A_1'$ and $\Gamma_B^- = A_1''$ are the symmetries with $+$ and $-$ parity, respectively, that are allowed by Bose–Einstein statistics for an XY_3 molecule, ND_3 say, whose Y nuclei are bosons.

The nuclear spin statistical weight factors g_{ns} for $^{14}NH_3$ are determined in Section 8.4.1 of Ref. [3] and we do not repeat the derivation here. The results are summarized in Table 2. The 24 nuclear spin functions (see Chapter 8 in Ref. [3]) of $^{14}NH_3$ span the representation

$$\Gamma_{\text{nspin}}^{\text{tot}} = 12A_1' \oplus 6E' \tag{29}$$

of D_{3h}(M). In Table 2, Γ_{rve} is the MS group symmetry of the rovibronic wavefunction $|\Phi_{\text{elec}}^{(w)}\rangle|\Phi_{\text{rv}}^{(w)}\rangle$, and for each possible Γ_{rve} we give under the heading 'Γ_{ns}' the number of spin functions available for forming complete internal wavefunctions of symmetry $\Gamma_{\text{int}} = \Gamma_F^+ = A_2'$ and $\Gamma_{\text{int}} = \Gamma_F^- = A_2''$, respectively, the total number of such spin functions equals the nuclear spin statistical weight

Table 2. Determination of statistical weight of the rovibronic states of $^{14}NH_3$ in the MS group D_{3h}(M) [3]

Γ_{rve}	Γ_{ns}	Γ_{int}	g_{ns}
A_1'	$-$; $-$	A_2'; A_2''	0
A_1''	$-$; $-$	A_2'; A_2''	0
A_2'	$12A_1'$; $-$	A_2'; A_2''	12
A_2''	$-$; $12A_1'$	A_2'; A_2''	12
E'	$6E'$; $-$	A_2'; A_2''	6
E''	$-$; $6E'$	A_1'; A_2''	6

factor $g_{\rm ns}$. We note that for $\Gamma_{\rm rve} = A_1'$ or A_1'', $g_{\rm ns} = 0$, so that the corresponding energy levels are *missing*. They do not exist because their rovibronic wavefunctions cannot be combined with nuclear spin functions in such a way as to obey Fermi–Dirac statistics.

We have [3]

$$\Gamma_{\rm rve} = \Gamma_{\rm elec} \otimes \Gamma_{\rm rv}, \tag{30}$$

where $\Gamma_{\rm elec}$ is the symmetry of $|\Phi_{\rm elec}^{(\rm w)}\rangle$ and $\Gamma_{\rm rv}$ is the symmetry of $|\Phi_{\rm rv}^{(\rm w)}\rangle$. We are concerned with the electronic ground state of NH_3 for which $\Gamma_{\rm elec} = A_1'$ so that for the rovibronic states of interest $\Gamma_{\rm rve} = \Gamma_{\rm rv}$. If $|\Phi_{\rm rv}^{(\rm i)}\rangle(|\Phi_{\rm rv}^{(\rm f)}\rangle)$ has the MS group symmetry $\Gamma_{\rm rv}''(\Gamma_{\rm rv}')$ then the line strength $S(\rm f \leftarrow i)$ can only be non-vanishing [3] if

$$\Gamma_{\rm rv}'' \otimes \Gamma_{\rm rv}' \supset \Gamma^* = A_1''. \tag{31}$$

In consequence, the symmetry selection rules on $\Gamma_{\rm rv}$ (with the corresponding $g_{\rm ns}$ values) are

$$A_2' \leftrightarrow A_2''; \quad g_{\rm ns} = 12 \tag{32}$$

$$E' \leftrightarrow E''; \quad g_{\rm ns} = 6. \tag{33}$$

These selection rules, in conjunction with the general rotational selection rules

$$\Delta J = J' - J'' = 0, \pm 1 \ \ (J'' + J' \geq 1) \tag{34}$$

determine the allowed electric dipole transitions of $^{14}NH_3$.

3. THE DIPOLE MOMENT FUNCTIONS

3.1. The *ab initio* calculation of the dipole moment

The NH_3 dipole moment surface used in the present study is obtained from two sets of *ab initio* data. As reported previously [4], the *ab initio* calculations were done at the CCSD(T)/aug-cc-pVTZ level of theory (i.e., coupled cluster theory with all single and double substitutions [23] and a perturbative treatment of connected triple excitations [24,25] with the augmented correlation-consistent triple-zeta basis [26,27]). The frozen-core approximation was applied. Dipole moments were computed by using a numerical finite-difference procedure with an added external dipole field of 0.005 a.u. The calculations employed the MOLPRO2000 [28,29] package. The convergence thresholds were 10^{-10} for density and 10^{-7} a.u. for energy in Hartree–Fock (HF) calculations, and 10^{-10} a.u. for energy and 10^{-10} for coefficients in CCSD(T) computations.

The first set of data was obtained on a two-dimensional grid (the 2D grid in Ref. [4]) consisting of 420 geometries of C_{3v} or D_{3h} symmetry, with bond distances $R_{\rm NH}$ between 0.60 and 1.65 Å, and angles $\alpha_{\rm HNH}$ between 70 and 120°. The data points were more dense in the vicinity of the equilibrium geometry and the saddle point. The second set of data was determined on a six-dimensional

grid (the 6D-1 grid in Ref. [4]) consisting of 14,400 unique geometries that form a regular grid in the range $0.85\ \text{Å} \leq r_1 \leq r_2 \leq r_3 \leq 1.20\ \text{Å}$ and $80° \leq \alpha_1 \leq \alpha_2 \leq \alpha_3 \leq 120°$.

The *ab initio* calculations give the components of the molecular dipole moment in a right-handed Cartesian axis system $x'y'z'$ with origin in the nitrogen nucleus. The H_1 nucleus lies on the z' axis with a positive value of the z' coordinate, and the plane defined by the nitrogen nucleus and the protons H_1 and H_2 is the $y'z'$ plane. Thus, in the $x'y'z'$ axis system, N has the coordinates (0,0,0), H_1 has the coordinates $(0,0,z_1')$ with $z_1' > 0$, H_2 has the coordinates $(0,y_2',z_2')$, and H_3 has the coordinates (x_3', y_3', z_3'). In general, all the coordinates y_2', z_2', x_3', y_3', and z_3' are different from zero.

3.2. The analytical representation of the dipole moment

The *ab initio* calculations produce values of $(\bar{\mu}_{x'}, \bar{\mu}_{y'}, \bar{\mu}_{z'})$, i.e., the components of the electronically averaged dipole moment along the $x'y'z'$ axes defined above. In order to calculate molecular line strengths, however, we must determine, as functions of the vibrational coordinates, the dipole moment components $(\bar{\mu}_x, \bar{\mu}_y, \bar{\mu}_z)$ along the molecule-fixed axes xyz (see equation (23)) defined by Eckart and Sayvetz conditions [1].

An *ab initio* calculation generally gives the components of the electronically averaged dipole moment in a *body-fixed* axis system such as the $x'y'z'$ system. For a body-fixed axis system, the orientation of the axes is determined directly from the instantaneous positions of the nuclei. So, for the $x'y'z'$ axis system, the z' axis lies along the NH_1 bond, and the $y'z'$ plane is the NH_1H_2 plane. The definition of the molecule-fixed axis system xyz is more complicated since it rests on the Eckart–Sayvetz conditions. The values of the Euler angles θ, ϕ, χ, which determine the orientation of the xyz axis system in space, are determined, together with the inversion coordinate ρ and the three centre-of-mass coordinates, by the solution of a system of seven coupled equations [1]. Consequently, in line strength calculations, we are required to transform the dipole moment from the body-fixed axis system $x'y'z'$, as used in the *ab initio* calculation, to the xyz axis system. In the present section, we discuss strategies for carrying out this transformation, and we discuss suitable analytical functions for representing the molecule-fixed components of the dipole moment.

In the papers on intensity calculations for triatomic molecules [18,19], which guide the present work, the body-fixed dipole moment components $(\bar{\mu}_{x'}, \bar{\mu}_{y'}, \bar{\mu}_{z'})$ are represented by parameterized analytical functions of geometrically defined coordinates (i.e., bond lengths and bond angles). The values of the parameters in these functions are determined by least-squares fittings to the *ab initio* points. The analytical functions $(\bar{\mu}_{x'}, \bar{\mu}_{y'}, \bar{\mu}_{z'})$ are then subjected to two transformations: One transforms from the $x'y'z'$ body-fixed system (called the xpq axis system in Ref. [19]) to the xyz molecule-fixed system, and the other transforms the dipole moment components from depending on the geometrically defined coordinates to depending on the coordinates that we have chosen to describe the vibrational motion. In our HBJ-inspired models for molecular rotation and vibration, these

coordinates are not geometrically defined. In Refs. [18,19] these two transformations are made, by a combination of analytical and numerical techniques, as part of the intensity calculation.

In the present work, we must carry out transformations of the dipole moment functions analogous to those described for triatomic molecules in Refs. [18,19]. Our approach to this problem is completely different from that made in Refs. [18,19]. We do not transform analytical expressions for the body-fixed dipole moment components $(\bar{\mu}_{x'}, \bar{\mu}_{y'}, \bar{\mu}_{z'})$. Instead we obtain, at each calculated *ab initio* point, discrete values of the dipole moment components $(\bar{\mu}_x, \bar{\mu}_y, \bar{\mu}_z)$ in the *xyz* axis system, and we fit parameterized, analytical functions of our chosen vibrational coordinates (see below) through these values. This approach has the disadvantage that we must carry out a separate fitting for each isotopomer of a molecule: Different isotopomers with the same geometrical structure have different *xyz* axis systems (because the Eckart and Sayvetz conditions depend on the nuclear masses) and therefore different dipole moment components $(\bar{\mu}_x, \bar{\mu}_y, \bar{\mu}_z)$. We resort to the approach of transforming the dipole moment at each *ab initio* point because the direct transformation of analytical expressions for the body-fixed dipole moment components $(\bar{\mu}_{x'}, \bar{\mu}_{y'}, \bar{\mu}_{z'})$ is not practicable for a four-atomic molecule. The fact that the four-atomic molecule has six vibrational coordinates causes a huge increase in the complexity of the transformations relative to that encountered for the triatomic molecules (with three vibrational coordinates) treated in Refs. [18,19].

By carrying out the transformation $(\bar{\mu}_{x'}, \bar{\mu}_{y'}, \bar{\mu}_{z'}) \rightarrow (\bar{\mu}_x, \bar{\mu}_y, \bar{\mu}_z)$ at each *ab initio* point separately and then fitting the resulting values of $(\bar{\mu}_x, \bar{\mu}_y, \bar{\mu}_z)$, we obtain a representation of the dipole moment tailor-made for computing the matrix elements $\langle V' | \bar{\mu}_m^{(1,\sigma)} | V'' \rangle$ $(\sigma = 0, \pm 1)$ entering into equation (21) in terms of the vibrational wavefunctions $|V\rangle$ employed in our model for the rotation and vibration of XY_3 molecules [1]. We would like, however, to make our NH_3 dipole moment surfaces generally available in a form independent of our particular choice of the molecule-fixed axis system *xyz*. We describe such a 'universal' representation of the electronically averaged dipole moment vector $\bar{\mu}$, the so-called *Molecular Bond (MB) representation*, in Section 3.2.1. From the MB expression for the dipole moment vector [equation (35)], the dipole moment components for *any* choice of the molecule-fixed axis system can be determined in terms of general, geometrically defined coordinates. In the sections following Section 3.2.1, we then return to the problem of calculating line strengths from equation (21), i.e., with our Eckart–Sayvetz choice of the molecule-fixed axis system *xyz*.

3.2.1. The molecular bond (MB) representation

We write $\bar{\boldsymbol{\mu}}$ in the form given in Refs. [30,31]:

$$\bar{\boldsymbol{\mu}} = \bar{\mu}_1^{\text{Bond}} \mathbf{e}_1 + \bar{\mu}_2^{\text{Bond}} \mathbf{e}_2 + \bar{\mu}_3^{\text{Bond}} \mathbf{e}_3 \tag{35}$$

where the three functions $\bar{\mu}_i^{\text{Bond}}$, $i = 1, 2, 3$, depend on the vibrational coordinates, and $\mathbf{e}_i$ is the unit vector along the N–H_i bond,

$$\mathbf{e}_i = \frac{\mathbf{r}_i - \mathbf{r}_4}{|\mathbf{r}_i - \mathbf{r}_4|} \tag{36}$$

with $\mathbf{r}_i$ as the position vector of nucleus i (the protons are labelled 1, 2, 3, and the nitrogen nucleus is labelled 4, see Fig. 1) in the xyz axis system. We see that the representation of the dipole moment in equation (35) is universal in the sense discussed above: The unit vectors $\mathbf{e}_i$ are defined in terms of the instantaneous positions of the nuclei and do not depend on a particular choice of the molecule-fixed axis system.

We have found that we can obtain a particularly accurate representation of the *ab initio* dipole moment values by introducing the projections

$$\bar{\mu}_i = \bar{\boldsymbol{\mu}} \cdot \mathbf{e}_i, \quad i = 1, 2, 3. \tag{37}$$

Inserting equation (35) in equation (37), we derive

$$\bar{\mu}_i = \bar{\boldsymbol{\mu}} \cdot \mathbf{e}_i = \sum_{j=1}^{3} \bar{\mu}_j^{\text{Bond}} (\mathbf{e}_j \cdot \mathbf{e}_i) = \sum_{j=1}^{3} A_{ij} \bar{\mu}_j^{\text{Bond}}, \tag{38}$$

where $A_{ij} = \mathbf{e}_j \cdot \mathbf{e}_i$ is an element of the non-orthogonal 3×3 matrix

$$\mathbf{A} = \begin{pmatrix} 1 & \cos\alpha_3 & \cos\alpha_2 \\ \cos\alpha_3 & 1 & \cos\alpha_1 \\ \cos\alpha_2 & \cos\alpha_1 & 1 \end{pmatrix}. \tag{39}$$

When the determinant $|\mathbf{A}| \neq 0$ we can invert $\mathbf{A}$ analytically and compute

$$\begin{pmatrix} \bar{\mu}_1^{\text{Bond}} \\ \bar{\mu}_2^{\text{Bond}} \\ \bar{\mu}_3^{\text{Bond}} \end{pmatrix} = \mathbf{A}^{-1} \begin{pmatrix} \bar{\mu}_1 \\ \bar{\mu}_2 \\ \bar{\mu}_3 \end{pmatrix}. \tag{40}$$

When the molecule is planar, i.e., when $\alpha_1 + \alpha_2 + \alpha_3 = 2\pi$, the determinant $|\mathbf{A}| = 0$ and $\mathbf{A}$ cannot be inverted. This is because in this particular situation, $\mathbf{e}_1$, $\mathbf{e}_2$, and $\mathbf{e}_3$ are linearly dependent and there are infinitely many possible values of $(\bar{\mu}_1^{\text{Bond}}, \bar{\mu}_2^{\text{Bond}}, \bar{\mu}_3^{\text{Bond}})$. In this case, we can express $\bar{\mu}$ in terms of $\mathbf{e}_1$ and $\mathbf{e}_2$ only [in that we set $\bar{\mu}_3^{\text{Bond}} = 0$ in equation (35)], and we can determine $\bar{\mu}_1^{\text{Bond}}$ and $\bar{\mu}_2^{\text{Bond}}$ in terms of $\bar{\mu}_1$ and $\bar{\mu}_2$.

The inversion operation E^* [3] in $D_{3h}(\text{M})$ has the effect of reversing the directions of $\bar{\boldsymbol{\mu}}$ and each of the $\mathbf{e}_i$: $E^* \bar{\boldsymbol{\mu}} = -\bar{\boldsymbol{\mu}}$ and $E^* \mathbf{e}_i = -\mathbf{e}_i$, $i = 1, 2, 3$. Therefore,

$$E^* \bar{\mu}_i = (-\bar{\boldsymbol{\mu}}) \cdot (-\mathbf{e}_i) = \bar{\mu}_i, \quad i = 1, 2, 3, \tag{41}$$

from equation (37). That is, $\bar{\mu}_i$ is invariant under E^* and we can write it in terms of the geometrically defined coordinates r_1, r_2, r_3, α_1, α_2, and α_3; these coordinates are all invariant under E^*. We define a new function $\bar{\mu}_0$ so that

$$\bar{\mu}_1 = \bar{\mu}_0(r_1, r_2, r_3, \alpha_1, \alpha_2, \alpha_3). \tag{42}$$

By making use of the fact that the permutation operations (123), (132), (12), (13), and (23) in D_{3h}(M) leave $\bar{\mu}$ unchanged [3], we derive the symmetry relations

$$\bar{\mu}_1 = \bar{\mu}_0(r_1, r_2, r_3, \alpha_1, \alpha_2, \alpha_3) = \bar{\mu}_0(r_1, r_3, r_2, \alpha_1, \alpha_3, \alpha_2), \tag{43}$$

$$\bar{\mu}_2 = \bar{\mu}_0(r_2, r_3, r_1, \alpha_2, \alpha_3, \alpha_1) = \bar{\mu}_0(r_2, r_1, r_3, \alpha_2, \alpha_1, \alpha_3), \tag{44}$$

$$\bar{\mu}_3 = \bar{\mu}_0(r_3, r_1, r_2, \alpha_3, \alpha_1, \alpha_2) = \bar{\mu}_0(r_3, r_2, r_1, \alpha_3, \alpha_2, \alpha_1). \tag{45}$$

Obviously all three functions $\bar{\mu}_1$, $\bar{\mu}_2$, and $\bar{\mu}_3$ are given in terms of $\bar{\mu}_0$, and we express this function as an expansion

$$\bar{\mu}_0 = \mu_0^{(0)} + \sum_k \mu_k^{(0)} \xi_k + \sum_{k,l} \mu_{k,l}^{(0)} \xi_k \xi_l + \sum_{k,l,m} \mu_{k,l,m}^{(0)} \xi_k \xi_l \xi_m + \sum_{k,l,m,n} \mu_{k,l,m,n}^{(0)} \xi_k \xi_l \xi_m \xi_n + \cdots, \tag{46}$$

where

$$\xi_k = r_k \exp(-\beta^2 r_k^2), \quad k = 1, 2, 3, \tag{47}$$

$$\xi_l = \cos(\alpha_{l-3}) - \cos\left(\frac{2\pi}{3}\right) = \frac{1}{2} + \cos(\alpha_{l-3}), \quad l = 4, 5, 6. \tag{48}$$

The expansion function is chosen such that $\bar{\mu}_0 = 0$ for ($r_1 = r_2 = r_3 = 0$, $\alpha_1 = \alpha_2 = \alpha_3 = 2\pi/3$). The factor $\exp(-\beta^2 r_k^2)$ is required to keep the expansion in equation (46) from attaining unreasonably large values at large r_i [31].

In the axis system $x'y'z'$ employed in the *ab initio* calculations, the N nucleus has the coordinates (0,0,0), and H_1 has the coordinates (0,0,z_1') with $z_1' > 0$. It follows from equation (36) that the unit vector $\mathbf{e}_1$ has the coordinates (0,0,1) in the $x'y'z'$ axis system and so

$$\bar{\mu}_1 = \bar{\mu}_0 = \bar{\boldsymbol{\mu}} \cdot \mathbf{e}_1 = \bar{\mu}_{z'} \tag{49}$$

where $\bar{\mu}_{z'}$ is obtained directly from the *ab initio* calculation. Therefore, in principle, it should be possible to obtain the values of the parameters defining the function $\bar{\mu}_0(r_1, r_2, r_3, \alpha_1, \alpha_2, \alpha_3)$ by fitting equation (46) through the computed values of $\bar{\mu}_{z'}$ only. However, we have made *ab initio* calculations at geometries for which $r_1 \leq r_2 \leq r_3$ always. If we simply fit the available, computed values of $\bar{\mu}_{z'}$, we are always fitting the projection of the dipole moment onto the *shortest* bond. This introduces an asymmetry which degrades the accuracy of our fitting. We could circumvent this problem by generating, for each *ab initio* point, the $\bar{\mu}_{z'}$ values at the 11 symmetrically equivalent points, to which the initial point is connected by operations $R \neq E$ in D_{3h}(M), and then fit all the resulting $\bar{\mu}_{z'}$ values. Another, equivalent way of circumventing the problem is to fit simultaneously the calculated values of $\bar{\mu}_1$, $\bar{\mu}_2$, and $\bar{\mu}_3$ at the original set of *ab initio* geometries with $r_1 \leq r_2 \leq r_3$. We have chosen the latter approach.

We fit equation (46) through the computed values of $\bar{\mu}_1$, $\bar{\mu}_2$, and $\bar{\mu}_3$ given by equations (43)–(45). It should be noted that the parameters in equation (46) are subject to constraints resulting from the fact that $\bar{\mu}_0(r_1, r_2, r_3, \alpha_1, \alpha_2, \alpha_3)$ is invariant to the simultaneous interchange of r_2 and r_3 and of α_2 and α_3 [equation (43)].

The expansion in equation (46), taken to fourth order, was fitted through the $3\times14{,}440$ *ab initio* dipole moment projections calculated for NH_3 at the CCSD(T)/aug-cc-pVTZ level of theory. In the fitting, we could usefully vary 91 parameters, and the root-mean-square (rms) deviation attained was 0.0006 D.[1] This is a remarkable fitting accuracy, compared to the 0.084 D attained in Ref. [31], where a much larger range of geometries was used. At the ATZfc *ab initio* equilibrium geometry [4] of $r_1=r_2=r_3=r_e=1.0149$ Å and $\alpha_1=\alpha_2=\alpha_3=\alpha_e=106.40°$, we calculate the 'equilibrium' dipole moment $\mu_e=1.5198$ D. The experimental value is (1.561 ± 0.005) D [32].

We have also checked the effect on the rms deviation of including higher order terms in equation (46). Extending the expansion in equation (46) to sixth order, we obtain an rms deviation of 0.00006 D in the fitting to the $3\times14{,}440$ *ab initio* dipole moment values. However, the number of parameters required is about 400, substantially more than with the fourth-order expansion. These results demonstrate the very high internal consistency (i.e., smoothness) of the *ab initio* dipole moment surface.

In spite of the fact that we have introduced the factor of $\exp(-\beta^2 r_i^2)$ in equation (47), our analytical expression for the dipole moment does not have a qualitatively correct asymptotic behaviour for the bond lengths $r_i \to \infty$. The function does not converge to the dipole moment of the NH_2 fragment if we 'remove' a hydrogen atom. However, neither does it diverge: The calculated dipole moment values at large r_i are around 2–3 D depending on which dissociation path we use. Obviously, the asymptotic behaviour of the dipole moment is of no importance for the simulations carried out in the present work; we are only concerned with molecular states well below dissociation.

3.2.2. The representation in the xyz axis system

In order that we can compute the matrix elements $\langle V'|\bar{\mu}_m^{(1,\sigma)}|V''\rangle$ ($\sigma=0, \pm1$), that enter into the expression for the line strength in equation (21), in terms of the vibrational basis functions $|V\rangle$ employed in our model for the rotation and vibration of XY_3 molecules [1], we must necessarily represent the electronically averaged dipole moment vector as

$$\bar{\boldsymbol{\mu}} = \bar{\mu}_x \mathbf{e}_x + \bar{\mu}_y \mathbf{e}_y + \bar{\mu}_z \mathbf{e}_z, \tag{50}$$

where $\mathbf{e}_x$, $\mathbf{e}_y$, $\mathbf{e}_z$ are unit vectors defining the orientations of the x, y, and z axes, respectively. These unit vectors are defined by the Eckart and Sayvetz conditions [1,3]. In the present section, we discuss how to obtain parameterized, analytical

[1] The fitted parameter values are available from the authors on request.

expressions for $(\bar{\mu}_x, \bar{\mu}_y, \bar{\mu}_z)$, given in terms of the vibrational coordinates that the vibrational wavefunctions $|V\rangle$ depend on.

3.2.2.1. The transformation of the ab initio dipole moment values to the xyz axis system

If we know the components of the electronically averaged dipole moment $(\bar{\mu}_X, \bar{\mu}_Y, \bar{\mu}_Z)$ in the space-fixed axis system *XYZ*, and we know the values of the Euler angles (θ, ϕ, χ) that define the orientation of the *xyz* axes relative to the *XYZ* axes (see, for example, Ref. [3]), we can compute the *xyz* components $(\bar{\mu}_x, \bar{\mu}_y, \bar{\mu}_z)$ of the dipole moment from the relations

$$\bar{\mu}_\alpha = \sum_{A=X,Y,Z} S_{\alpha,A}(\theta, \phi, \chi)\bar{\mu}_A, \quad \alpha = x, y, z, \tag{51}$$

where the $S_{\alpha,A}(\theta,\phi,\chi)$ are the elements of an orthogonal, 3×3 transformation matrix **S** (see, for example, Refs. [3,33]). We determine the values of (θ, ϕ, χ) from the equation expressing the coordinate transformation from the *xyz* to the *XYZ* axis system [1]:

$$R_{i,A} = R_A^{\mathrm{CM}} + \sum_{\alpha=x,y,z} (\mathbf{S}^{-1})_{A,\alpha}(\theta, \phi, \chi)\left[a_{i,\alpha}(\rho) + \sum_{\lambda=1,2,3,4a,4b} A_{i\alpha,\lambda}(\rho)S_\lambda^\ell\right], \tag{52}$$

In equation (52), $R_{i,A}$ $(A=X, Y, Z)$ is the A-coordinate of the position vector for nucleus i, and R_A^{CM} is the A-coordinate of the nuclear centre of mass. $(\mathbf{S}^{-1})_{A,\alpha}(\theta, \phi, \chi)$ is an element of $\mathbf{S}^{-1}$, the elements of the ρ-dependent matrix $A_{i\alpha,\lambda}(\rho)$ are defined in Ref. [1], whereas the α-coordinate $a_{i\alpha}(\rho)$ $(\alpha=x, y, z)$ of nucleus i in the HBJ reference configuration [1] is given in Ref. [34]. The HBJ inversion coordinate ρ is defined in Ref. [1]. When the molecule is in the reference configuration, which has C_{3v} or D_{3h} geometrical symmetry (i.e., it has $r_1=r_2=r_3=r_e$ and $\alpha_1=\alpha_2=\alpha_3$), ρ is the angle between the C_3 rotational symmetry axis and any one of the N–H bonds. That is, $0\leq\rho\leq\pi$ (see Ref. [1] and Fig. 1). Finally, in equation (52), the S_λ^ℓ are the linearized coordinates defined in Ref. [1]; these coordinates measure the displacement of the molecule from the reference configuration. For $\lambda=1$, 2, 3 we have $S_\lambda^\ell = r_\lambda^\ell - r_e$, where $r_\lambda^\ell \approx r_\lambda$ when the molecule is near the reference configuration. Further,

$$S_{4a}^\ell = \frac{1}{\sqrt{6}}(2\alpha_1^\ell - \alpha_2^\ell - \alpha_3^\ell), \tag{53}$$

$$S_{4b}^\ell = \frac{1}{\sqrt{2}}(\alpha_2^\ell - \alpha_3^\ell). \tag{54}$$

where $\alpha_i^\ell \approx \alpha_i$ when the molecule is near the reference configuration.

At each calculated *ab initio* point we set the space-fixed *XYZ* axis system equal to the $x'y'z'$ axis system employed in the *ab initio* calculations. That is, we set $(R_{i,X}, R_{i,Y}, R_{i,Z})=(x_i', y_i', z_i')$ for $i=1$, 2, 3, 4. We then use least-squares methods to determine from equation (52) a set of 12 coordinates ρ, R_X^{CM}, R_Y^{CM}, R_Z^{CM}, θ, ϕ, χ, S_1^ℓ, S_2^ℓ, S_3^ℓ, S_{4a}^ℓ, S_{4b}^ℓ (to any desired accuracy). These coordinate values

will, by necessity, satisfy the Eckart and Sayvetz conditions [1]; this is ensured by the form of the matrix elements $A_{i\alpha,\lambda}(\rho)$ [1]. With the computed values of θ, ϕ, χ, and the known *ab initio* values of $(\bar{\mu}_X, \bar{\mu}_Y, \bar{\mu}_Z) = (\bar{\mu}_{x'}, \bar{\mu}_{y'}, \bar{\mu}_{z'})$, we can then compute $(\bar{\mu}_x, \bar{\mu}_y, \bar{\mu}_z)$ from equation (51).

3.2.2.2. The analytical representations of $(\bar{\mu}_x, \bar{\mu}_y, \bar{\mu}_z)$

We fit analytical functions of ρ, S_1^ℓ, S_2^ℓ, S_3^ℓ, S_{4a}^ℓ, and S_{4b}^ℓ through the values of $(\bar{\mu}_x, \bar{\mu}_y, \bar{\mu}_z)$ resulting from the transformation described above. The analytical representation of $\bar{\mu}_\alpha$ $(\alpha = x, y, z)$ is chosen as

$$\bar{\mu}_\alpha(\xi_1^\ell, \xi_2^\ell, \xi_3^\ell, \xi_{4a}^\ell, \xi_{4b}^\ell; \rho) = \mu_0^\alpha(\rho) + \sum_k \mu_k^\alpha(\rho)\xi_k^\ell + \sum_{k\le l} \mu_{kl}^\alpha(\rho)\xi_k^\ell\xi_l^\ell + \sum_{k\le l\le m} \mu_{klm}^\alpha(\rho)\xi_k^\ell\xi_l^\ell\xi_m^\ell + \sum_{k\le l\le m\le n} \mu_{klmn}^\alpha(\rho)\xi_k^\ell\xi_l^\ell\xi_m^\ell\xi_n^\ell \cdots \tag{55}$$

by analogy with the Type B representation of the potential energy surface defined in Ref. [1]. In equation (55) we have introduced the linearized variables

$$\xi_k^\ell = 1 - \exp(-aS_k^\ell), \quad k = 1, 2, 3, \tag{56}$$

$\xi_{4a}^\ell = S_{4a}^\ell$, $\xi_{4b}^\ell = S_{4b}^\ell$, and the range parameter a occurring in the analytical representation for the potential energy function [1]. The quantities ξ_1^ℓ, ξ_2^ℓ, ξ_3^ℓ, ξ_{4a}^ℓ, and ξ_{4b}^ℓ are discussed further in Ref. [1].

The ρ-dependent functions $\mu_{kl\ldots}^\alpha(\rho)$ ($\alpha = x$ or y) in equation (55) are chosen as

$$\mu_{kl\ldots}^\alpha(\rho) = \sum_{s\ge 0} \mu_{kl\ldots}^{\alpha(s)}(\sin\rho_0 - \sin\rho)^s, \quad 0 \le \rho \le \pi, \tag{57}$$

where we take $\rho_0 = \pi/2$, corresponding to the planar configuration. The dipole moment components $(\bar{\mu}_x, \bar{\mu}_y)$ have E' symmetry in $D_{3h}(M)$ and therefore ($\alpha = x$ or y)

$$E^* \mu_{kl\ldots}^\alpha(\rho) = \mu_{kl\ldots}^\alpha(\rho) \tag{58}$$

or, equivalently,

$$\mu_{kl\ldots}^\alpha(\pi - \rho) = \mu_{kl\ldots}^\alpha(\rho) \tag{59}$$

since $E^*\rho = \pi - \rho$. The function $\mu_{kl\ldots}^\alpha(\rho)$ given in equation (57) satisfies this requirement.

The dipole moment component $\bar{\mu}_z$ has A_2'' symmetry in $D_{3h}(M)$ so that

$$\mu_{kl\ldots}^z(\pi - \rho) = -\mu_{kl\ldots}^z(\rho). \tag{60}$$

We choose ($\rho_0 = \pi/2$)

$$\mu_{kl\ldots}^z(\rho) = \sum_{s>0} \mu_{kl\ldots}^{z(s)}(\cos\rho_0 - \cos\rho)^s \quad \text{for } \frac{\pi}{2} \le \rho \le \pi, \tag{61}$$

and

$$\mu^z_{kl\ldots}(\rho) = -\mu^z_{kl\ldots}(\pi - \rho) \quad \text{for } 0 \leq \rho < \frac{\pi}{2}. \tag{62}$$

Since, with the definition in equation (61), $\mu^z_{kl\ldots}(\pi/2) = 0$, no inconsistency arises because of equation (62). If we allowed only odd powers s in the sum of equation (61), we could let this equation define $\mu^z_{kl\ldots}(\rho)$ in the entire interval $0 \leq \rho \leq \pi$. However, we have found that a better fit to the *ab initio* dipole moment values can be obtained when we include both odd and even s in equation (61) and extend the definition by equation (62).

Equations (59) and (62) ensure that the analytical representations of $(\bar{\mu}_x, \bar{\mu}_y, \bar{\mu}_z)$ have the correct transformation properties under the inversion operation E^*. Since the appropriate symmetry group for NH_3, $D_{3h}(M)$, can be written as the direct product given in equation (27), we must now ascertain that $(\bar{\mu}_x, \bar{\mu}_y, \bar{\mu}_z)$ also transform appropriately under the operations in $C_{3v}(M)$. If this is the case, they will have correct transformation properties under all operations in $D_{3h}(M)$.

Correlation from $D_{3h}(M)$ to $C_{3v}(M)$ shows that $(\bar{\mu}_x, \bar{\mu}_y)$ have E symmetry in $C_{3v}(M)$ and $\bar{\mu}_z$ has A_1 symmetry. We investigate the transformation properties of $(\bar{\mu}_x, \bar{\mu}_y, \bar{\mu}_z)$ in $C_{3v}(M)$ by means of a newly developed MAPLE VI [35] routine.[2] By definition [3], the effect of a symmetry operation R in $C_{3v}(M)$ on the dipole moment component $\bar{\mu}_\alpha(\xi^\ell_k)$ is given by

$$R\bar{\mu}_\alpha(\xi^\ell_k) = \bar{\mu}_\alpha(R\xi^\ell_k), \tag{63}$$

where ξ^ℓ_k is a shorthand notation for all the variables ξ^ℓ_1, ξ^ℓ_2, ξ^ℓ_3, ξ^ℓ_{4a}, ξ^ℓ_{4b}, and we omit the coordinate ρ which is invariant under the operations in $C_{3v}(M)$. For example, since $\bar{\mu}_z$ has A_1 symmetry in $C_{3v}(M)$, it is left unchanged by the operation $(23)^*$:

$$(23)^*\bar{\mu}_z(\xi^\ell_1, \xi^\ell_2, \xi^\ell_3, \xi^\ell_{4a}, \xi^\ell_{4b}) = \bar{\mu}_z(\xi^\ell_1, \xi^\ell_2, \xi^\ell_3, \xi^\ell_{4a}, \xi^\ell_{4b}). \tag{64}$$

On other hand, it is straightforward to determine the effect of $(23)^*$ on the variables ξ^ℓ_1, ξ^ℓ_2, ξ^ℓ_3, ξ^ℓ_{4a}, ξ^ℓ_{4b}:

$$(23)^*\bar{\mu}_z(\xi^\ell_1, \xi^\ell_2, \xi^\ell_3, \xi^\ell_{4a}, \xi^\ell_{4b}) = \bar{\mu}_z(\xi^\ell_1, \xi^\ell_3, \xi^\ell_2, \xi^\ell_{4a}, -\xi^\ell_{4b}). \tag{65}$$

Comparison of equations (64) and (65) produces

$$\bar{\mu}_z(\xi^\ell_1, \xi^\ell_2, \xi^\ell_3, \xi^\ell_{4a}, \xi^\ell_{4b}) = \bar{\mu}_z(\xi^\ell_1, \xi^\ell_3, \xi^\ell_2, \xi^\ell_{4a}, -\xi^\ell_{4b}). \tag{66}$$

When we now insert the expansion from equation (55) on both sides of equation (66), relations between the expansion coefficients in equation (55) ensue. For example, from equation (66) the first-order expansion coefficients in the expression for $\bar{\mu}_z$ must satisfy

$$\mu^{z(s)}_2 = \mu^{z(s)}_3 \tag{67}$$

[2] This routine is available from the authors on request.

$$\mu_{4a}^{z(s)} = -\mu_{4a}^{z(s)} \tag{68}$$

so that $\mu_{4a}^{z(s)} = 0$. By combining these relations with the results of applying other C_{3v}(M) operations, we obtain that to first order

$$\bar{\mu}_z = \mu_0^z(\rho) + \mu_1^z(\rho)(\xi_1^\ell + \xi_2^\ell + \xi_3^\ell). \tag{69}$$

Relations for the higher order parameters $\mu_{klmn\ldots}^{\alpha}$ (up to sixth order) are derived analytically using the MAPLE command 'solve', which arbitrarily chooses a minimum set of independent parameters and expresses the other parameters in terms of them. The derived relations are then converted to FORTRAN and become part of the intensity program. Analogous MAPLE procedures have also been applied for the dipole moment function in the MB representation and for the potential function expansions [1].

3.2.2.3. The least-squares fitting of $(\bar{\mu}_x, \bar{\mu}_y, \bar{\mu}_z)$

Having derived the symmetry relations between the expansion parameters in equation (55), we can proceed to fit the expansions through the *ab initio* dipole moment values. The expansion parameters in the expressions for $\bar{\mu}_x$ and $\bar{\mu}_y$ are connected by symmetry relations since these two quantities have E' symmetry in D_{3h}(M), and so $\bar{\mu}_x$ and $\bar{\mu}_y$ must be fitted together. The component $\bar{\mu}_z$, with A_2'' symmetry, can be fitted separately. The variables ξ_k^ℓ, ρ in equation (55) are chosen to reflect the properties of the potential surface, rather than those of the dipole moment surfaces. Therefore, the fittings of $(\bar{\mu}_x, \bar{\mu}_y, \bar{\mu}_z)$ require more parameters than the fittings of the MB dipole moment representations. We fitted the 14,400 *ab initio* data points using 77 parameters for the $\bar{\mu}_z$ component and 141 parameters for $\bar{\mu}_x$, $\bar{\mu}_y$. The rms deviations attained were 0.00016 and 0.0003 D, respectively.

The parameterized, analytical representations of $(\bar{\mu}_x, \bar{\mu}_y, \bar{\mu}_z)$ determined in the fitting are in a form suitable for the calculation of the vibronic transition moments $\langle V'|\bar{\mu}_m^{(1,\sigma)}|V''\rangle$ ($\sigma = 0, \pm 1$), that enter into the expression for the line strength in equation (21). These matrix elements are computed in a manner analogous to that employed for the matrix elements of the potential energy function in Ref. [1].

4. APPLICATIONS

4.1. Transition moments

In this section, we report calculated values of the vibrational transition moments for vibrational transitions $v_2'v_2^{\mp} \leftarrow v_2''v_2^{\pm}$ of $^{14}NH_3$, where ν_2 is the inversion mode,[3] $v_2'' \leq 4$ and $v_2' \leq 4$. These transition moments are matrix elements of $\bar{\mu}_z$; they are essentially determined by the dependence of $\bar{\mu}_z$ on the inversion coordinate ρ.

[3] In the labelling of the vibrational states, a superscript + indicates the lower (symmetric) inversion component; the upper (antisymmetric) component is indicated by a superscript −.

The transition moments are calculated from the *ab initio* dipole moment surface, represented in the *xyz* axis system as described above. They are defined as

$$\mu_{\mathrm{fi}} = \sqrt{\sum_{\alpha=x,y,z} |\langle \Phi_{\mathrm{rv}}^{(\mathrm{f})} | \bar{\mu}_\alpha | \Phi_{\mathrm{rv}}^{(\mathrm{i})} \rangle|^2}, \tag{70}$$

where $\bar{\mu}_\alpha$ is given in equation (55), while $|\Phi_{\mathrm{rv}}^{(\mathrm{i})}\rangle$ and $|\Phi_{\mathrm{rv}}^{(\mathrm{f})}\rangle$ are the $J=0$ rotation–vibration functions computed variationally as described in Ref. [1]. As mentioned above, for the vibrational transitions that we consider here, only matrix elements of $\bar{\mu}_z$ are non-vanishing in equation (70). The wavefunctions $|\Phi_{\mathrm{rv}}^{(\mathrm{i})}\rangle$ and $|\Phi_{\mathrm{rv}}^{(\mathrm{f})}\rangle$ are obtained from the *ab initio* potential energy surface CBS**-5 [36]. This surface is determined as follows: ATZfc electronic energies were computed at 51,816 nuclear geometries using the CCSD(T) method (coupled cluster theory with all single and double substitutions [23] and a perturbative treatment of connected triple excitations [24,25]) with the augmented correlation-consistent triple-zeta basis aug-cc-pVTZ [26,27]. At 3814 selected geometries, more accurate CBS+ energies were determined by extrapolating the CCSD(T) results to the complete basis set limit and including corrections for relativistic effects and core–valence correlation [4]. The differences between the ATZfc and CBS+ energies were fitted by a sixth-order polynomial in geometrically defined, internal coordinates, and the corrections were added to the ATZfc energies at all 51,816 grid points to generate the CBS**-5 surface (which is close to CBS+ quality). An analytical representation of this surface was obtained by fitting the sixth-order expansion given in equation (7) of Ref. [4] through all CBS**-5 data points. The resulting 181 potential parameter values will be given elsewhere [36] and are also available from the authors on request.

In the variational calculations, the expansions of the kinetic energy factors $G_{\alpha\beta}$ and the pseudo-potential U [1] are taken to fourth order, and, as mentioned above, the potential energy V is expanded through sixth order. In the numerical integration of the inversion Schrödinger equation a grid of 1000 points is used. The basis set [1] is truncated so that

$$P = 2(v_1 + v_2 + v_3) + v_{\mathrm{inv}} + v_4 \leq 14. \tag{71}$$

With $P \leq 14$, the $J=0$ matrix blocks corresponding to A_1 and E symmetry in the group $C_{3v}(\mathrm{M})$ have the dimensions $N(A_1)=1455$ and $N(E)=2571$, respectively. The matrices are diagonalized with routines from the LAPACK library [37].

The calculated transition moments are listed in Table 3, where they are compared with the available experimental data [38–44] and also with the values calculated by Marquardt *et al.* [31] and Pracna *et al.* [45]. Our results are in good agreement with both the experimental and the theoretical data.

There is a qualitative change in the dependence of the $\Delta v_2 = 1$ transition moments on the inversion state at the top of the barrier to planarity, which is about 1800 cm^{-1} [4,46–50]. Below the inversion barrier, the matrix elements $\langle (v_2-1)^+ | \bar{\mu}_z | v_2^- \rangle$ and $\langle (v_2-1)^- | \bar{\mu}_z | v_2^+ \rangle$ are approximately equal. Above the barrier

Table 3. Transition moments (in D) for vibrational transitions $v_2'\nu_2^{\mp} \leftarrow v_2''\nu_2^{\pm}$ of $^{14}NH_3$

$(v_2'')^{\pm}$	$(v_2')^{\pm}$	Obs.	References[a]	Reference [45]	Reference [31]	Present work
0^+	1^-	0.236	[38]	0.237	0.208	0.235
0^-	1^+	0.248	[38]	0.247	0.218	0.245
1^+	2^-	0.285	[39]	0.287	0.270	0.286
1^-	2^+			0.525	0.508	0.514
2^+	3^-			0.111	0.083	0.112
2^-	3^+	1.05	[40]	0.901	0.943	0.888
3^+	4^-					0.034
3^-	4^+					0.993
0^+	0^-	1.4719	[41]	1.471	1.574	1.456
1^+	1^-	1.2448	[42]	1.248	1.355	1.238
2^+	2^-	1.02	[40]	0.948	1.047	0.938
3^+	3^-			0.981	1.039	0.967
4^+	4^-			1.043	1.072	1.020
0^+	2^-	0.0033	[43]	0.000	0.026	0.003
0^-	2^+	0.0204	[43]	0.019	0.009	0.020
0^+	3^-	0.0037	[44][b]	0.005	0.016	0.003
0^-	3^+	0.0060	[44][b]	0.008	0.026	0.005
0^+	4^-					0.001
0^-	4^+					0.002

[a] Reference for the observed value given under the heading 'Obs.'
[b] Benedict *et al.* [44] as cited in Ref. [45].

(i.e., for $v_2 > 2$) the $\langle (v_2-1)^+|\bar{\mu}_z|v_2^-\rangle$ transition moment is much smaller than $\langle (v_2-1)^-|\bar{\mu}_z|v_2^+\rangle$. We explain this behaviour by means of wavefunction analysis.

First we note that, as shown in Fig. 2, $|\bar{\mu}_z|$ is zero at planar configurations and increases with inversion displacement. Consequently, a large value of

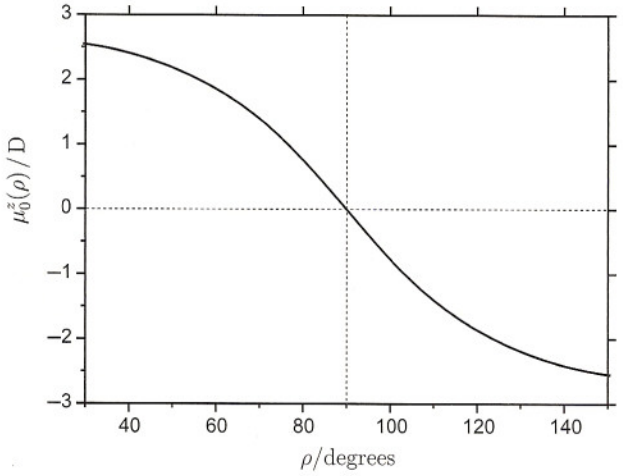

Fig. 2. The function $\mu_0^z(\rho)$ for $^{14}NH_3$. Note that $\mu_0^z(\pi-\rho) = -\mu_0^z(\rho)$.

the transition moment $\langle (v_2'')^{\pm}|\bar{\mu}_z|(v_2')^{\mp}\rangle$ requires that the two wavefunctions $|(v_2'')^{\pm}\rangle$ and $|(v_2')^{\mp}\rangle$ have a significant overlap at distorted geometries with ρ near 0 or ρ near π. To investigate how the wavefunctions overlap, we plot in Fig. 3 the inversion angle probability distribution, obtained by integrating the square of the vibrational wavefunction over the stretching and small-amplitude bending coordinates S_1^{ℓ}, S_2^{ℓ}, S_3^{ℓ}, S_{4a}^{ℓ}, and S_{4b}^{ℓ}, for states $v_2 v_2^{\pm}$ with $v_2 \leq 4$. The normalized inversion-coordinate probability density function $f(\rho)$ is given by

$$f(\rho) = \int \mathrm{d}V |\psi_{\mathrm{vib}}|^2, \tag{72}$$

where $\mathrm{d}V$ is the volume element for the stretching and small-amplitude bending coordinates S_1^{ℓ}, S_2^{ℓ}, S_3^{ℓ}, S_{4a}^{ℓ}, and S_{4b}^{ℓ}.

In Fig. 3, the states $v_2 v_2^{\pm}$ are combined in pairs $[(v_2-1)^{\pm}, v_2^{\mp}]$ corresponding to the vibrational transitions in Table 3. At $v_2 \leq 2$ (i.e., below the inversion barrier), the figure shows that for each of the two wavefunction pairs $[(v_2-1)^{-}, v_2^{+}]$ and $[(v_2-1)^{+}, v_2^{-}]$, the pair members overlap in a similar manner and have significant comparable overlaps for ρ near 0 or ρ near π. At higher v_2 values, the members of the $[(v_2-1)^{-}, v_2^{+}]$ pair overlap only at very distorted geometries with ρ near 0 or ρ near π. The corresponding transition moments are therefore large. The members of the $[(v_2-1)^{+}, v_2^{-}]$ pair overlap near planarity ($\rho \approx \pi/2$), where $|\bar{\mu}_z|$ is small, and so the corresponding transition moments are small. These wavefunctions are dephased for ρ near 0 or ρ near π. Thus, the qualitative variation of $[(v_2-1)^{-}, v_2^{+}]$ and $[(v_2-1)^{+}, v_2^{-}]$ with excitation of the inversion mode is connected with the fact that the amplitude of the inversion wavefunctions is shifted away from the planar configuration, i.e., it is shifted towards $\rho=0$ or $\rho=\pi$, in higher excited inversion states.

4.2. Simulations of rotation–vibration spectra

As detailed in Section 2, we have derived and programmed the expression for line strengths of individual rotation–vibration transitions of XY_3 molecules; the line strengths depend on the vibronic transition moments entering into equation (70). With the theory of Section 2, we can simulate rotation–vibration absorption spectra of XY_3 molecules. In computing the transition wavenumbers, line strengths, and intensities we use rovibronic wavefunctions generated as described in Ref. [1].

In the present section, we give examples of simulated vibrational bands of $^{14}NH_3$. These bands start in the lowest inversion states $0^{\pm}$ and end in the states $v_2 v_2^{\mp}$ with $v_2 \leq 4$. The rovibrational wavefunctions with $J \leq 18$ are calculated variationally as described in Ref. [1]. To make these variational calculations feasible the size of the vibrational basis set is reduced relative to that employed for the calculations of vibrational transition moments in Section 4.1. We now require that

$$P = 2(v_1 + v_2 + v_3) + v_{\mathrm{inv}} + v_4 \leq 8. \tag{73}$$

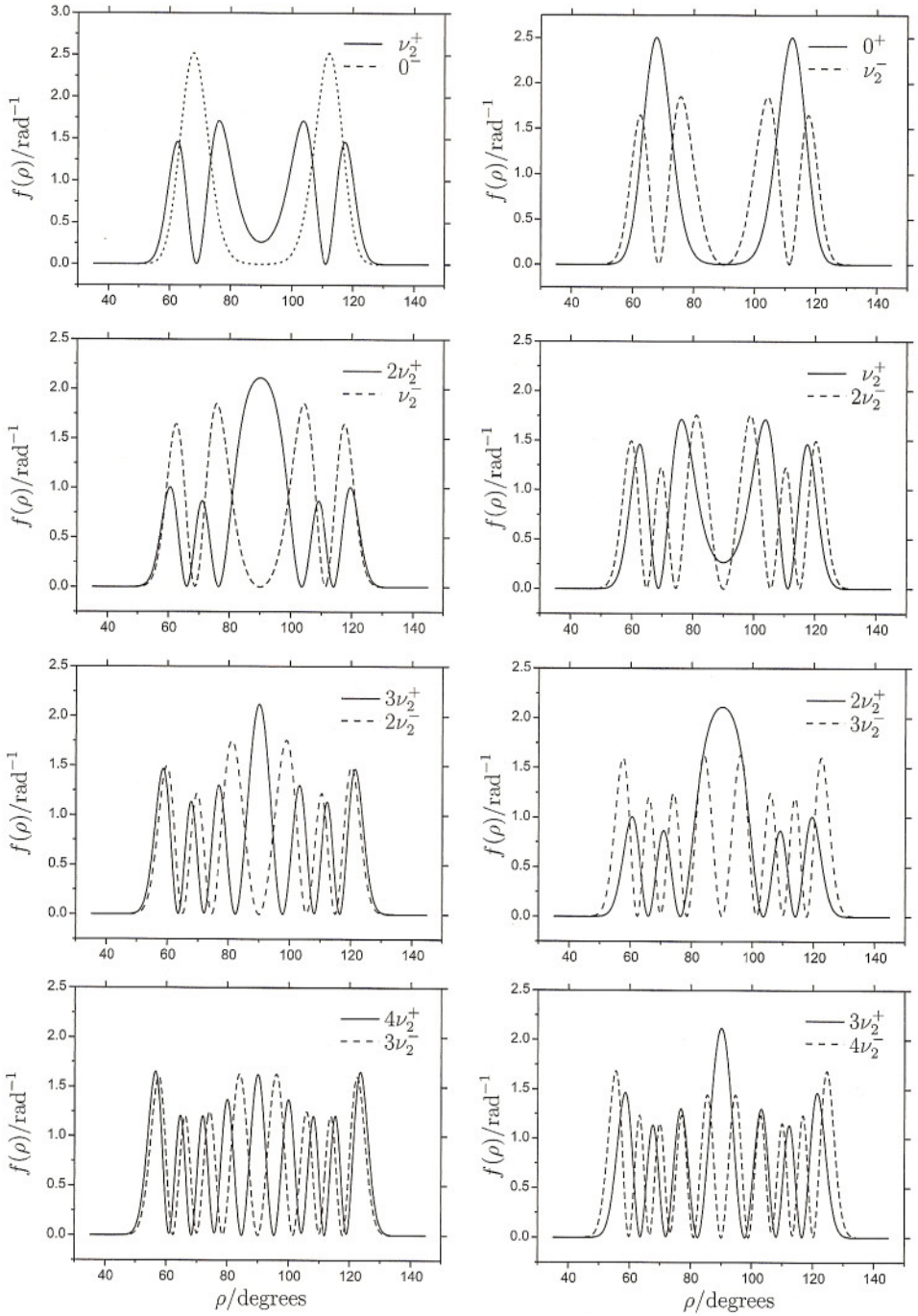

Fig. 3. Inversion probability density functions for the $^{14}NH_3$ inversion states $\upsilon_2\nu_2^{\pm}$ with $\upsilon_2 \leq 4$.

The largest matrix blocks obtained with this basis set are the E symmetry blocks at $J=18$; they have the dimension $N(E)=9150$.

In Fig. 4, we show simulations of the vibrational absorption bands $\upsilon_2'\nu_2^{\pm} \leftarrow 0^{\pm}(\upsilon_2' \leq 4)$ for $^{14}NH_3$. The simulated spectra are drawn as stick diagrams where the height of the stick representing a line is the integrated absorption coefficient from equation (6), calculated from the line strengths given by equation (21) at the absolute temperature $T=295$ K. In these calculations, we use the partition function value $Q=1713.33$, which is obtained from the $J \leq 18$ term

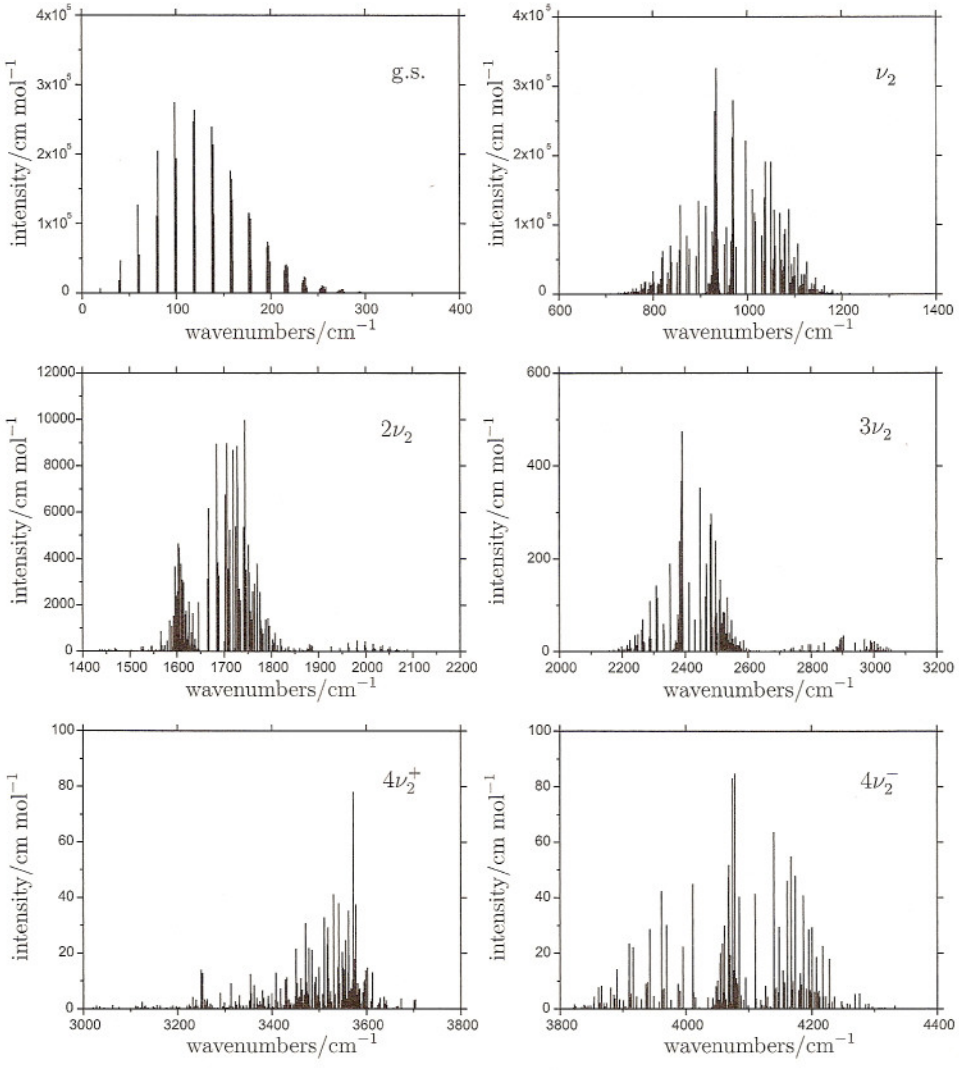

Fig. 4. Simulations of the vibrational absorption bands $\upsilon_2'\nu_2^{\mp} \leftarrow 0^{\pm}(\upsilon_2' \leq 4)$ for $^{14}NH_3$ at the absolute temperature $T=295$ K. The plots for ν_2, $2\nu_2$, and $3\nu_2$ comprise the two components $\upsilon_2'\nu_2^{+} \leftarrow 0^{-}$ and $\upsilon_2'\nu_2^{-} \leftarrow 0^{+}$.

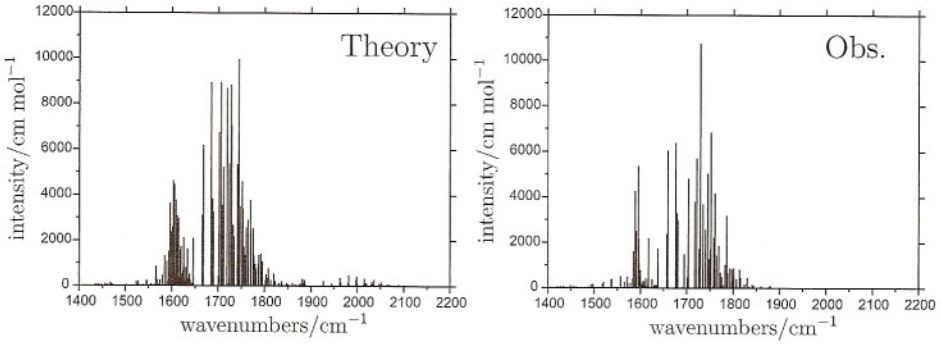

Fig. 5. Simulations of the $2\nu_2$ and ν_4 bands of $^{14}NH_3$ at $T=295$ K compared to experimental data from Ref. [43].

values calculated variationally below 6000 cm^{-1} and the spin statistical weight factors for $^{14}NH_3$ from Table 2. This value of Q can be compared to the value of 574.16 from Ref. [51], obtained at $T=295$ K with spin statistical weight factors which, in an obvious notation, can be written as $g_{ns}(A_1)=0$, $g_{ns}(A_2)=4$, and $g_{ns}(E)=2$. That is, the spin statistical weights employed in Ref. [51] are three times smaller than those given in Table 2. The reason is that Urban *et al.* [51] ignore the factor of 3 which the ^{14}N nucleus (with spin $I=1$) contributes to each nuclear spin statistical weight factor. This difference does not matter for the calculation of the integrated absorption coefficient $I(f\leftarrow i)$ from equation (6) since the line strength factor $S(f\leftarrow i)$ in this equation contains a factor of g_{ns} [equation (21)], while all terms in the partition function Q also contain g_{ns}-factors. Multiplying all g_{ns}-values by a constant factor thus does not change $I(f\leftarrow i)$. In the present work, we follow Bunker and Jensen [3] in defining g_{ns} as the actual nuclear-spin degeneracy of each rotation–vibration level, and this leads to the g_{ns}-values in Table 2. When we multiply the Q value from Ref. [51] by 3, we get $Q=1722.48$, in satisfactory agreement with the value of 1713.33 from the present work.

In the simulated band $4\nu_2^{\pm}\leftarrow 0^{\pm}$ in Fig. 4, both components ($+\leftarrow -$ and $-\leftarrow +$) have comparable intensities, whereas in the bands $2\nu_2^{\pm}\leftarrow 0^{\pm}$ and $3\nu_2^{\pm}\leftarrow 0^{\pm}$ the $+\leftarrow -$ component dominates as suggested by the transition moments in Table 3.

To assess the quality of the simulated spectra, we compare in Fig. 5 the simulated $2\nu_2$ and ν_4 bands of $^{14}NH_3$ with stick spectra drawn with the experimental data given in appendix of Ref. [43]. That is, the 'experimental' spectrum shows only the transitions *assigned* in Ref. [43], which explains why the experimental spectrum contains less lines than the simulated one. In the simulated and the 'experimentally derived' stick spectra, the intensities are given as integrated absorption coefficients in cm mol^{-1}. The experimental values, originally [43] given in cm^{-2} atm^{-1}, were converted to cm mol^{-1} at $T=295$ K. We see that there is significant similarity between the simulated and 'experimentally derived' stick spectra: The agreement with experiment is rather good.

5. CONCLUSIONS

In the present paper, we have described a complex, but powerful 'tool' for simulating spectra of NH_3. The simulated spectra are directly comparable with experimentally observed spectra. The tool consists of

- a variationally based model, with accompanying computer program, for accurate calculations of rovibrational energies and wavefunctions of XY_3 pyramidal molecules [1],
- an accurate *ab initio* potential energy function for NH_3 [36],
- a computational procedure for intensity simulations based on the results of the variational calculations [Section 2.3, in particular equation (21)], and
- high quality *ab initio* dipole moment surfaces for NH_3.

The accuracy of the dipole moment surfaces is documented by the calculated transition moments in Table 3.

In Fig. 5, the agreement of the calculated absolute intensity values with the corresponding experimental values is an indication of the high quality of the *ab initio* dipole moment surfaces employed in the calculation. The qualitatively correct appearance of the bands indicates that our solution of the rotation–vibration Schrödinger equation and the potential energy surface employed are satisfactory. It should be emphasized that the *ab initio* potential energy and dipole moment surfaces have not been adjusted to fit experiment.

ACKNOWLEDGEMENTS

The initial stages of this work were supported by the European Commission through contract no. HPRN-CT-2000-00022 'Spectroscopy of Highly Excited Rovibrational States'. The final stages were also supported by the European Commission (contract no. MRTN-CT-2004-512202 'Quantitative Spectroscopy for Atmospheric and Astrophysical Research'). The work of PJ is supported in part by the Deutsche Forschungsgemeinschaft and the Fonds der chemischen Industrie.

REFERENCES

[1] S. N. Yurchenko, M. Carvajal, P. Jensen, H. Lin, J. Zheng and W. Thiel, *Mol. Phys.*, 2005, **103**, 359.
[2] J. T. Hougen, P. R. Bunker and J. W. C. Johns, *J. Mol. Spectrosc.*, 1970, **34**, 136.
[3] P. R. Bunker and P. Jensen, *Molecular Symmetry and Spectroscopy*, 2nd edn., NRC Research Press, Ottawa, 1998.
[4] H. Lin, W. Thiel, S. N. Yurchenko, M. Carvajal and P. Jensen, *J. Chem. Phys.*, 2002, **117**, 11265.
[5] S. N. Yurchenko, M. Carvajal, P. Jensen, F. Herregodts and T. R. Huet, *Chem. Phys.*, 2003, **290**, 59.
[6] D. Wang, Q. Shi and Q.-S. Zhu, *J. Chem. Phys.*, 2000, **112**, 9624.

[7] C. Léonard, N. C. Handy, S. Carter and J. M. Bowman, *Spectrochim. Acta A*, 2002, **58**, 825.
[8] S. M. Colwell, S. Carter and N. C. Handy, *Mol. Phys.*, 2003, **101**, 523.
[9] S. N. Yurchenko, P. R. Bunker and P. Jensen, *J. Mol. Struct.*, 2005, **742**, 43.
[10] L. Lammich, H. Buhr, H. Kreckel, S. Krohn, M. Lange, D. Schwalm, R. Wester, A. Wolf, D. Strasser, D. Zajfman, Z. Vager, I. Abril, S. Heredia-Avalos and R. Garcia-Molina, *Phys. Rev. A*, 2004, **69**, 062904.
[11] F. Légaré, K. F. Lee, I. V. Litvinyuk, P. W. Dooley, S. S. Wesolowski, P. R. Bunker, P. Dombi, F. Krausz, A. D. Bandrauk, D. M. Villeneuve and P. Corkum, *Phys. Rev. A*, 2005, **71**, 013415.
[12] P. Jensen, T. E. Odaka, W. P. Kraemer, T. Hirano and P. R. Bunker, *Spectrochim. Acta A*, 2002, **58**, 763.
[13] S. N. Yurchenko, W. Thiel, S. Patchkovskii and P. Jensen, Contributed Lecture M3, 18th International Conference on High Resolution Molecular Spectroscopy, Prague, Czech Republic, September 8–12, 2004.
[14] S. N. Yurchenko, W. Thiel, S. Patchkovskii and P. Jensen, *Phys. Chem. Chem. Phys.* 2005, **7**, 573.
[15] P. Jensen, G. Osmann and I. N. Kozin, in *Vibration–Rotational Spectroscopy and Molecular Dynamics* (ed. D. Papoušek), World Scientific, Singapore, 1997.
[16] P. Jensen, *Mol. Phys.*, 2000, **98**, 1253.
[17] I. Kleiner, L. R. Brown, G. Tarrago, Q.-L. Kou, N. Picqué, G. Guelachvili, V. Dana and J.-Y. Mandin, *J. Mol. Spectrosc.*, 1999, **193**, 46.
[18] P. Jensen and V. Špirko, *J. Mol. Spectrosc.*, 1986, **118**, 208.
[19] P. Jensen, *J. Mol. Spectrosc.*, 1988, **132**, 429.
[20] S. S. Penner, *Quantitative Molecular Spectroscopy and Gas Emissivities*, Addison-Wesley, Reading, MA, 1959.
[21] G. K. Woodgate, *Elementary Atomic Structure*, McGraw-Hill, Maidenhead, 1970.
[22] R. N. Zare, *Angular Momentum*, Wiley, New York, 1988.
[23] G. D. Purvis and R. J. Bartlett, *J. Chem. Phys.*, 1982, **76**, 1910.
[24] M. Urban, J. Noga, S. J. Cole and R. J. Bartlett, *J. Chem. Phys.*, 1985, **83**, 4041.
[25] K. Raghavachari, G. W. Trucks, J. A. Pople and M. Head-Gordon, *Chem. Phys. Lett.*, 1989, **157**, 479.
[26] T. H. Dunning, *J. Chem. Phys.*, 1989, **90**, 1007.
[27] D. E. Woon and T. H. Dunning, *J. Chem. Phys.*, 1993, **98**, 1358.
[28] MOLPRO2000 is a package of *ab initio* programs written by H.-J. Werner and P. J. Knowles, with contributions from R. D. Amos, A. Bernhardsson, A. Berning, P. Celani, D. L. Cooper, M. J. O. Deegan, A. J. Dobbyn, F. Eckert, C. Hampel, G. Hetzer, T. Korona, R. Lindh, A. W. Lloyd, S. J. McNicholas, F. R. Manby, W. Meyer, M. E. Mura, A. Nicklass, P. Palmieri, R. Pitzer, G. Rauhut, M. Schütz, H. Stoll, A. J. Stone, R. Tarroni and T. Thorsteinsson.
[29] C. Hampel, K. Peterson and H.-J. Werner, *Chem. Phys. Lett.*, 1992, **190**, 1 and references therein. The program to compute the perturbative triples corrections has been developed by M. J. O. Deegan and P. J. Knowles, *Chem. Phys. Lett.*, 1994, **227**, 321.
[30] S.-G. He, J.-J. Zheng, S.-M. Hu, H. Lin, Y. Ding, X.-H. Wang and Q.-S. Zhu, *J. Chem. Phys.*, 2001, **114**, 7018.
[31] R. Marquardt, M. Quack, I. Thanopulos and D. Luckhaus, *J. Chem. Phys.*, 2003, **119**, 10724.
[32] M. D. Marshall, K. C. lzgi and J. S. Muenter, *J. Chem. Phys.*, 1997, **107**, 1037.
[33] D. Papoušek and M. R. Aliev, *Molecular Vibrational–Rotational Spectra*, Elsevier, Amsterdam, 1982.
[34] D. Papoušek, J. M. R. Stone and V. Špirko, *J. Mol. Spectrosc.*, 1973, **48**, 17.
[35] M. B. Monagan, K. O. Geddes, K. M. Heal, G. Labahn, S. M. Vorkoetter and J. McCarron, Maple 6 Programming Guide, Waterloo Maple, Toronto, 2000.
[36] H. Lin, J. J. Zheng, S. N. Yurchenko, P. Jensen and W. Thiel, to be published.
[37] E. Anderson, Z. Bai, C. Bischof, S. Blackford, J. Demmel, J. Dongarra, J. Du Croz, A. Greenbaum, S. Hammarling, A. McKenney and D. Sorensen, LAPACK Users' Guide, http://www.netlib.org/lapack/, 3rd edn., 1999.
[38] T. Nakanaga, S. Kondo and S. Saëki, *J. Mol. Spectrosc.*, 1985, **112**, 39.
[39] P. H. Beckwith, D. J. Danagher and J. Reid, *J. Mol. Spectrosc.*, 1987, **121**, 209.
[40] M. Takami, H. Jones and T. Oka, *J. Chem. Phys.*, 1979, **70**, 3557.

[41] K. Tanaka, H. Ito and T. Tanaka, *J. Chem. Phys.*, 1987, **87**, 1557.
[42] Y. Ueda and J. Iwahori, *J. Mol. Spectrosc.*, 1986, **116**, 191.
[43] C. Cottaz, I. Kleiner, G. Tarrago, L. R. Brown, J. S. Margolis, R. L. Poynter, H. M. Pickett, T. Fouchet, P. Drossart and E. Lellouch, *J. Mol. Spectrosc.*, 2000, **203**, 285.
[44] W. S. Benedict, E. K. Plyler and E. D. Tidwell, *J. Chem. Phys.*, 1958, **29**, 829.
[45] P. Pracna, V. Špirko and W. P. Kraemer, *J. Mol. Spectrosc.*, 1989, **136**, 317.
[46] T. Rajamäki, A. Miani and L. Halonen, *J. Chem. Phys.*, 2003, **118**, 10929.
[47] J. Pesonen, A. Miani and L. Halonen, *J. Chem. Phys.*, 2001, **115**, 1243.
[48] C. Léonard, S. Carter and N. C. Handy, *Chem. Phys. Lett.*, 2003, **370**, 360.
[49] A. G. Császár, W. D. Allen and H. F. Schaefer III., *J. Chem. Phys.*, 1998, **108**, 9751.
[50] W. Klopper, C. C. M. Samson, G. Tarczay and A. G. Császár, *J. Comput. Chem.*, 2001, **22**, 1306.
[51] Š Urban, D. Papoušek, V. M. Devi, B. Fridovich, R. D'Cunha and K. N. Rao, *J. Mol. Spectrosc.*, 1984, **106**, 38.